ALFRED-WEGENER-INSTITUT
HELMHOLTZ-ZENTRUM FÜR POLAR- UND MEERESFORSCHUNG

Universität Bremen

Carbon cycling in an Arctic fjord (Scoresby Sund, East Greenland) with regard to the influence of glacial meltwater discharge

Master Thesis in Marine Biology

Submitted by

Miriam Seifert

March 2018

First supervisor: Dr. Morten Hvitfeldt Iversen
Second supervisor: Dr. Tim Rixen
together with Dr. Mario Hoppema

Abstract

Greenland fjords receive considerable amounts of meltwater discharge from the Greenland Ice Sheet, influencing the physical and biogeochemical conditions within the fjords. Because ice melt will increase with ongoing climate change, research on present-day conditions is urgently needed to make better projections for the future. In the present study, a comprehensive analysis of the carbon cycle in Scoresby Sund, the world's largest fjord system situated at the southeastern coast of Greenland, was conducted.

In summer 2016, Scoresby Sund and its northernmost branch, Nordvestfjord, were visited. While the narrow Nordvestfjord is influenced by numerous marine-terminating glaciers and surface meltwater discharge, the wide Outer Scoresby Sund is much less affected by meltwater. Surface partial pressure of CO_2, primary production, particulate organic carbon (POC) flux, and remineralisation within the water column are reported. The data reveal that meltwater significantly influenced the carbon dynamics within the fjord. First, meltwater itself increased the uptake of carbon dioxide from the atmosphere. Second, meltwater limited net community production in Nordvestfjord to 31 - 35 mmol C m^{-2} d^{-1} compared to the Outer Scoresby Sund and the shelf (43 - 67 mmol C m^{-2} d^{-1}) by inhibiting the resupply of nutrients to the surface and by shadowing of silts contained in the meltwater. Finally, the POC flux close to glacier fronts was enhanced due to ballasting by silts, which diminished the remineralisation within the water column and increased the share of organic carbon that reached the sea floor. In Outer Scoresby Sund, by contrast, most remineralisation took place in the upper water column and particle concentrations below were mainly dependent on the present water mass.

This study presents the first findings ever about biogeochemical cycling in Scoresby Sund. The results imply that Greenland fjords should be examined on a regional scale to highlight significant differences in carbon dynamics depending on the degree of meltwater discharge within a single fjord system.

Zusammenfassung

Das Grönländische Eisschild versorgt Grönlands Fjorde mit beträchtlichen Mengen an Schmelzwasser, welches sowohl die physikalischen als auch die biogeochemischen Bedingungen in den Fjorden beeinflusst. Da der fortwährende Klimawandel zu einer Zunahme der Eisschmelze führt, sind Untersuchungen der derzeitigen Bedingungen dringend notwendig, um bessere Vorhersagen für die Zukunft machen zu können.

In der vorliegenden Forschungsarbeit wurde eine umfassende Analyse des Kohlenstoffkreislaufs im Scoresby Sund, dem weltweit größten Fjordsystem an der Südostküste Grönlands, durchgeführt.

Im Sommer 2016 fand eine Expedition in den Scoresby Sund und seinen nördlichsten Fjordarm, den Nordvestfjord, statt. Während der schmale Nordvestfjord von einer Vielzahl an marin endenden Gletschern und oberflächlichen Schmelzwasserflüssen geprägt ist, ist der Einfluss von Schmelzwasser auf den breiten äußeren Scoresby Sund um einiges geringer. Untersucht wurde der oberflächliche Partialdruck von CO_2, die Primärproduktion, der Fluss an partikulärem organischen Kohlenstoff (POC) und die Remineralisierung in der Wassersäule. Die Daten zeigen, dass die Dynamik im Kohlenstoffkreislauf erheblich vom Schmelzwasser geformt wird. Schmelzwasser selbst verstärkte die Aufnahme von atmosphärischem Kohlenstoffdioxid in das Fjordwasser. Die Netto-Gemeinschaftsproduktion im Nordvestfjord wurde durch das Schmelzwasser auf 31 - 35 mmol C m^{-2} d^{-1} im Vergleich zum äußeren Scoresby Sund und dem Schelf mit 43 - 67 mmol C m^{-2} d^{-1} limitiert, da die Versorgung des Oberflächenwassers mit Nährstoffen verhindert wurde und Schlickpartikel im Schmelzwasser die Lichteinstrahlung reduzierten. Darüber hinaus wurde der vertikale POC-Fluss in der Nähe von Gletscherfronten durch das höhere Gewicht der Schlickpartikel verstärkt, wodurch die Remineralisierung der Partikel in der Wassersäule verringert wurde und ein größerer Anteil des POCs den Fjordboden erreichte. Im äußeren Scoresby Sund dagegen fand die Remineralisierung großteils in der oberen Wassersäule statt und die Partikelkonzentration darunter war hauptsächlich von der vorherrschenden Wassermasse abhängig.

Diese Forschungsarbeit dokumentiert die ersten Untersuchungen zu biogeochemischen Kreisläufen im Scoresby Sund. Die Ergebnisse zeigen, dass die Grönländischen Gletscher im regionalen Maßstab untersucht werden sollten, um entscheidende Unterschiede in der Kohlenstoffdynamik abhänging vom Ausmaß des Schmelzwasserausflusses innerhalb eines Fjordsystems herauszustellen.

Contents

Chapter 1

Introduction

While modelling the carbon cycle of the whole Arctic Ocean seems to be challenging, if not even impossible (reviewed by *Findlay et al.*, 2015), the key to get a better understanding of the fate of atmospheric carbon dioxide in the Arctic realm lies in studying smaller and defined regions. The facts that Arctic fjords are exposed to an increasing amount of meltwater and that fjords in general seem to be an important site for carbon burial (*Smith et al.*, 2015), makes them to one of the most interesting areas for studying the carbon cycle. In the following study, the largest fjord system of the world, Scoresby Sund, which is situated on the eastern side of Greenland, is examined regarding the fixation of carbon in biological biomass, the transport of this biomass to depth, and the remineralisation back into inorganic carbon within the water column. These processes are embedded in information about the physical setting within the fjord, giving a snapshot of the situation during summer 2016. As comparable data from this fjord are lacking to date, this study is hoped to contribute to the overall picture of the carbon cycling in Arctic regions.

1.1 Climate change in the Arctic and effects on the Greenland Ice Sheet

Atmospheric carbon dioxide (CO_2) concentrations have been rising by about 120 ppm since pre-industrial times and are thought to rise strongly further, because of the enormous emissions of anthropogenic CO_2 due to fossil fuel combustion and land use change (*IPCC*, 2014). *Notz and Stroeve* (2016) observed a linear relationship between the cumulative anthropogenic CO_2 emissions and the size of the Arctic sea ice area. The authors believe, however, that due to the increasing sensitivity of the Arctic marine realm to changes in oceanic heat content, this linearity will no longer be given, and that the remainder of the Arctic summer sea ice will be lost before

mid-21st century.

The Greenland Ice Sheet (GrIS) has an estimated size of $2.96 \cdot 10^6$ km^2, of which about 22% are below sea level. If the whole ice sheet would melt, it would have the potential to raise the global mean sea level by about 8 m (*Bamber et al.*, 2013). Indeed, a substantial thinning of the GrIS has occurred since 2006, triggered by regional warming of the surrounding waters (*Khan et al.*, 2014). The mass loss of the GrIS from 1992 to 2011 led to a sea level rise of 7.5 mm, which makes up 1/4 of the present global sea level rise (reviewed by *Straneo and Cenedese*, 2015), and is thought to progress with a rate of more than 10 Gt yr^{-1} in the northeastern part of the ice sheet (*Khan et al.*, 2014). Beside the effects on the global sea level, increasing freshening of the waters around Greenland could alter or weaken the Atlantic Meridional Overturning circulation (*Yang et al.*, 2016).

Greenland's glacial fjords are an essential link between the GrIS mass loss and the open ocean, as most of the meltwater is discharged and modified within the fjord waters before entering the large-scale ocean. Greenland fjords are characterized by deep sills, which let Atlantic as well as Arctic water from the shelves enter (reviewed by *Straneo and Cenedese*, 2015). These waters are mixed with freshwater from glacial discharge, originating either from land- or marine-terminating glaciers. This results in complex circulation patterns, affecting the physical, biological, and biogeochemical processes alongside the extentions of the fjords.
Until now, however, only few studies have examined the carbon cycling in Arctic fjords while considering both physical and biological parameters (e.g., *Rysgaard et al.*, 2012; *Meire et al.*, 2015; *Sørensen et al.*, 2015). For east Greenland, most work has been conducted as part of a long-term monitoring programme in the northeastern Greenland fjord Young Sound (e.g., *Rysgaard et al.*, 1998; *Glud et al.*, 2002; *Rysgaard et al.*, 2003; *Rysgaard and Nielsen*, 2006; *Glud and Rysgaard*, 2007; *Sejr et al.*, 2011; *Meire et al.*, 2016a, 2017). In 75 years, the conditions in this fjord are projected to resemble present-day conditions in Scoresby Sund, which is ~450 km further south (*Rysgaard and Glud*, 2007). A thorough examination of the carbon cycling in Scoresby Sund does, therefore, not only reveal the impact of the global climate on Arctic fjords, but may also generate a model system to show the expected conditions in more northerly regions where increased ice-melting is expected within the next decades (*Rysgaard et al.*, 2003). Thus, a broader understanding of the carbon dynamics in fjords concerning physical and chemical parameters is of urgent need.

1.2 Factors determining the fjord's carbon dynamics

1.2.1 The influence of meltwater on fjord CO_2 uptake dynamics

Because of their cold temperatures and low salinities, Arctic waters are vulnerable to take up CO_2 from the atmosphere, which is then transported to depth via deep water formation. *Lauderdale et al.* (2016) identified the northeast and high-latitude Atlantic Ocean to be a sink for atmospheric CO_2. However, also outgassing disequilibrium fluxes can occur. For the whole Arctic Ocean, there are still discussions ongoing whether, and to what extent, it will continue to act as a CO_2 sink in the future (*Bates et al.*, 2006; *Cai et al.*, 2010) as many factors come into play, such as the stratification due to surface warming, the scope of primary productivity, and the residence time of surface waters. Therefore, each region of the Arctic Ocean should be evaluated separately (*Yasunaka et al.*, 2016). The prospective situation in Arctic fjords is, however, barely considered. Present-day measurements show that during summer, meltwater at the inner side of glacially influenced fjords and wind fetch together with tidal mixing at the fjord mouth lead to a net uptake of atmospheric CO_2 (e.g., *Sejr et al.*, 2011; *Rysgaard et al.*, 2012; *Meire et al.*, 2015; *Reisdorph and Mathis*, 2015).

During winter, the extent of ice coverage is an important factor determining the degree of air-sea gas exchange. During ice formation, the resulting cold brine below the newly formed ice has an enhanced gas solubility. Due to its higher density, the gas enriched water sinks to depth and is replaced by undersaturated water at the surface (*Anderson et al.*, 2004). Ice cover itself, though, hampers air-sea gas exchange, and also an only partially ice covered sea surface takes up less CO_2 than expected from a linear scaling to percent ice cover, possibly because of reduced wind fetch (*Rutgers van der Loeff et al.*, 2014).

Fjord systems that are connected to glacier termini are, in addition to the meltwater from sea ice, influenced by glacier meltwater discharge. Most of this discharge occurs at the grounding line of the glaciers through discharge outlets rather than at the surface (*Fried et al.*, 2015; *Straneo and Cenedese*, 2015), running a buoyancy-driven circulation within the fjord. During this circulation, meltwater plumes rise towards the surface and are replaced by warmer water coming from the shelf, leading to the advection of oceanic heat towards the glacier (*Sciascia et al.*, 2013; *Cowton et al.*, 2016; *Stevens et al.*, 2016). This in turn can then enhance the meltwater runoff by destabilizing the glacier front. Besides, the melt of icebergs within the fjord is regarded as a sink for oceanic heat as well as an additional source of liquid freshwater (*Enderlin et al.*, 2016; *Moon et al.*, 2017).
Meltwater from glacial discharge can contribute to surface water undersaturation

and the concomitant uptake of atmospheric CO_2 by being itself undersaturated in CO_2, or by the non-conservative mixing behaviour of fresh and saline water, resulting in low CO_2 partial pressure (pCO_2) (*Mook and Koene*, 1975; *Meire et al.*, 2015).
A correlation between surface pCO_2 and salinity could be found in several studies (*Rysgaard et al.*, 2012; *Fransson et al.*, 2013; *Meire et al.*, 2015), leading to the assumption that meltwater is one of the driving factors establishing the flux of CO_2 into the sea.

1.2.2 The fate of CO_2 in seawater

The carbon dioxide system in the ocean is made up by three carbon species: CO_2*(aq), which is the sum of all unionized carbon dioxide (CO_2(aq) and H_2CO_3(aq)), bicarbonate (HCO_3^-(aq)), and carbonate (CO_3^{2-}(aq)). The concentrations of these species cannot be measured directly. To overcome this problem, mainly four variables are determined: total dissolved inorganic carbon (DIC), total alkalinity (TA), fugacity of CO_2 (fCO_2, which is pCO_2 corrected for non-ideality due to the interaction with other gases), and total hydrogen ion concentration (usually defined as pH = -log[H^+]) (*Dickson et al.*, 2007). At least two of these variables should be measured to evaluate the complete carbon dioxide system of a relevant marine area. In many cases, DIC and TA are chosen, as their determination with present-day methods can be highly precise and accurate (*Mintrop et al.*, 2000). DIC is defined as the total molecular concentration of CO_2*, HCO_3^-, and CO_3^{2-}. While different definitions of TA exist, this study assesses TA as excess of proton acceptors over proton donators in 1 kg of sample seawater. For this, carbonates as well as the major ions borate and phosphate were considered:
$TA = [HCO_3^+] + 2[CO_3^{2-}] + [OH^-] + [HPO_4^{2-}] + 2[PO_4^{3-}] - [H^+] - [H_3PO_3]$.
Nitrate as an anion of a strong acid is not part of this equation, because over the titration range, no protons are exchanged (*Wolf-Gladrow et al.*, 2007).

The distribution of DIC and TA on a vertical scale as well as along transects indicate physical and biological dynamics within the ocean. For example, sea ice dynamics can result in a five times larger seasonal amplitude of the carbonate-system parameters in the upper 2 m compared to the upper 20 m of the water column (*Fransson et al.*, 2013).

DIC is changed as soon as uptake of atmospheric CO_2 occurs. Sea ice formation at the surface can cause a DIC excess at depth, when cold, CO_2-enriched brine sinks (*Anderson et al.*, 2004). *Ulfsbo et al.* (2014) report that the DIC concentration along their cruise track mirrored the salinity distribution. Additionally, the DIC content of a watermass can indicate its age (*Wanninkhof et al.*, 2013).
By contrast, TA is often considered as a conservative parameter. Non-conservative

TA behaviour can be caused by dilution or evaporation and sea ice formation, as well as biochemical processes involving carbonate minerals (*Friis et al.*, 2003). Also the amount of organic compounds and the degree of denitrification can, although to a minor extent, have an effect on TA (*Brewer and Goldman*, 1976; *Cross et al.*, 2013). Usually, TA values are corrected for changes in salinity, organic compounds, and denitrification. Then the remaining non-conservative behaviour indicates either the presence of carbonate-forming organisms or the introduction of reactive carbonate minerals (*Anderson et al.*, 2004; *Sejr et al.*, 2011; *Rysgaard et al.*, 2012; *Cross et al.*, 2013; *Ulfsbo et al.*, 2014). If glacial runoff is low in TA, it can reduce the buffering capacity of the surrounding seawater against changes in pH (*Reisdorph and Mathis*, 2014).

1.2.3 The biological contribution to seawater carbon dynamics

The uptake of atmospheric CO_2 into the sea water is not only enhanced by physical processes such as meltwater undersaturation, wind fetch, and circulation, but also by the drawdown of dissolved CO_2 through photosynthetic processes. During photosynthesis, inorganic carbon is stored in organic compounds, building up the biomass of organisms. High primary productivity can help to keep local pCO_2 levels in the surface waters low, as observed in the west Greenland fjord Godthåbsfjord (*Rysgaard et al.*, 2012). It is possible that primary productivity will increase with ongoing climate change due to increased light availability, resulting from the decrease in ice coverage, intensified upwelling, and enhanced import of nutrients together with shelf waters (*Rysgaard and Glud*, 2007; *Murray et al.*, 2015). Glacial melt, however, introduces particles (*Murray et al.*, 2015), which then again tend to impede primary productivity by light attenuation. Predicting the presence and magnitude of a phytoplankton bloom within a fjord is therefore difficult, resulting in only a few publications about Greenland fjord's primary production (e.g., *Juul-Pedersen et al.*, 2015; *Meire et al.*, 2016b, 2017).

The net community production (NCP) is defined as the gross primary production minus all losses in carbon due to respiration, and can be seen as a proxy for the fraction of primary production that will be exported to a depth below the surface layer (export production) (*Williams*, 1993; *Hansell and Carlson*, 1998; *Lee*, 2001). It can either be obtained by satellite image analyses, or by accounting for the change in the budget of a relevant reactant that is part of the photosynthetic process. Another method which is, however, barely used by other authors, is to estimate NCP by the accumulation of products like dissolved organic matter (*Hansell and Carlson*, 1998). Satellite-based NCP determinations can cover a larger area, but can add significant errors when depth integration is made inaccurately (*Munro et al.*, 2015). Thus, ground truthing of the satellite data is crucial, making budget-based NCP

determinations necessary. For that, DIC, pCO_2, and nutrient concentrations can be used (*Hoppema et al.*, 2007; *Ulfsbo et al.*, 2014).
Accounting for some uncertainties coming along with these methods, they result in relatively good NCP estimates. *Anderson et al.* (2003) determined an export production of 0.5 g C m^{-2} yr^{-1} for the central Arctic Ocean.

1.2.4 Particulate organic carbon flux and remineralisation

During autotrophic production, carbon dioxide is fixed in organic compounds via photosynthesis. These organic compounds are grazed by heterotrophic organisms and are transferred through the food chain. By packing into fecal pellets or through physical aggregation of small particles, the organic carbon forms larger sinking particles that gradually sink out of the surface ocean to greater depths. Particles $> 500\,\mu m$ are commonly known as marine snow. On its way down through the water column, the marine snow is either consumed by zooplankton, remineralised by microbes and other organisms which respire and release the carbon as CO_2, or is buried in the ocean sediments (reviewed by *Alldredge and Silver*, 1988).

To determine this flux of particulate organic carbon (POC) in the water column, a closer look has to be taken onto the particle dynamics. Generally, the number of large particles decreases considerably with depth (*Karakaş et al.*, 2009). This is mainly due to high disaggregation within the upper meters of the water column (*Iversen et al.*, 2010). Additionally, minerals, which might for example enter the water column with glacial melt, can even enhance disaggregation (*Iversen and Robert*, 2015; *Lalande et al.*, 2016). Next to the particle size, the speed with which particles are sinking defines the magnitude of the POC flux. Sinking velocities of differently sized particles are mainly determined by their sources and age, and the ballasting by minerals (*Ploug et al.*, 2008; *Iversen et al.*, 2010; *Iversen and Robert*, 2015), and are therefore directly linked to the prevailing marine environment. Thus, they cannot be compared globally (*Nowald et al.*, 2009). To identify local features in the POC flux, like the influence of glacial meltwater discharge, it is crucial to estimate the POC flux on a small scale.
What additionally comes into play, next to the inorganic (dis)aggregation and ballasting, is the remineralisation of organic compounds by organisms. Faecal pellets, for instance, are mainly degraded by protozooplankton in the upper water column (*Poulsen and Iversen*, 2008), whereas microbial degradation is higher in deeper water layers. This might result in earlier remineralisation of one nutrient to another.
If additional POC is advected into the region in question, for example by terrestrial runoff or by advection from the surrounding sea, the total POC flux will not correlate with the magnitude of primary production in the surface layer (*McMahon and*

Patching, 1984; *Rysgaard and Nielsen*, 2006; *Sørensen et al.*, 2015).

Organic material which is not remineralised within the water column reaches the sea floor. Benthic remineralisation removes some of this organic matter from the sediment. However, a fraction of it is permanently buried on the ocean floor. In the east Greenland fjord Young Sound, for example, 48% of the carbon entering the sediment is preserved through burial (*Rysgaard et al.*, 1998). This carbon is then the only one which is permanently removed from exchange with the atmosphere. Fjords play a significant role in the organic carbon burial as their burial rate is, per unit area, one hundred times larger than the global ocean average (*Smith et al.*, 2015). *Sørensen et al.* (2015) expect that with longer ice-free periods, the benthic remineralisation and burial will increase.

1.3 Objectives

The aim of this study is to investigate the carbon system of a high-Arctic fjord, Scoresby Sund (east Greenland), by compiling data from physical, biological, and chemical measurements. As the sampling was conducted within a transect from the inner fjord to the fjord mouth, the dataset will also give an insight into the influence of glacial meltwater and water from the Greenland Sea on oceanographic parameters. Furthermore, this study intends to demonstrate the possible future conditions in fjords further north.
Besides giving a broad insight into the oceanographic conditions in Scoresby Sund, the following objectives will be particularly addressed in the present study:

Objective 1: How does the carbonate system (DIC, TA, pCO_2) change with distance to the glaciers?
Hypothesis 1: The inflow of meltwater might lead to an undersaturation in CO_2. A high export production lowers DIC, which could be the case at the outer fjord as the introduction of nutrients from the Greenland Sea could enhance primary production. Besides, DIC distribution is influenced by air-sea gas exchange (affected by fresher meltwater next to the glacial outflow) and transport processes (e.g., inflow of water from the Greenland Sea). TA might be higher in areas influenced by glacial meltwater due to the latter's high load of reactive carbonate minerals.

Objective 2: Determination of the net community production: Is the productivity of the system and, thus, the export production significantly different with distance to the glaciers?
Hypothesis 2: The NCP largely depends on light and nutrient availability. As the

inflowing water from the adjacent Greenland Sea might import nutrients and the ice cover decreases with distance from the glaciers, NCP likely increases towards the fjord mouth. Additionally, glacial runoff containing terrestrial sediment particles could have a shadowing effect on the upper water column and hence limit primary productivity.

Objective 3: Determination of the POC flux and the remineralisation rate with depth: Is all organic matter from the export production remineralized within the water column or does a fraction of it reach the sea floor?
Hypothesis 3: Fjords are known to bury carbon in relatively high amounts. The sediment-loaded glacial runoff does enhance vertical biomass flux due to ballasting (*Iversen and Robert*, 2015; *Wiedmann et al.*, 2016). Additionally, the adjacent shelf area could be a source of additional carbon. Thus, it is hypothesized that a significant fraction of the organic carbon produced at the surface is remineralised or buried in the fjord sediments.

Chapter 2

Materials and Methods

2.1 Study area

Scoresby Sund at the eastern coast of Greenland is the largest fjord system in the world, covering an area of 13,700 km^2 with a total distance of 350 km between the head of the inner fjord and the mouth. A high mountain plateaux 1500-2000 m above sea level dominates the innermost part of the Scoresby Sund region. The eastwards extending continental shelf has a width of 80-100 km until the shelf break at approximately 500 m depth. The fjord itself is divided into two parts: the wide, outer fjord with a maximum depth of 650 m, and the narrow inner fjords, including Gaasefjord, Fønfjord, Øfjord, and Nordvestfjord. The inner fjords are characterised by a complex topography and steep slopes, with water depths of up to 1500 m (*Funder*, 1972; *Dowdeswell et al.*, 1993; *Cofaigh et al.*, 2001). Fast-flowing outlet glaciers cover a considerably larger coastal area of the inner fjords in comparison to the outer fjord (*Cofaigh et al.*, 2001). During the study of *Dowdeswell et al.* (1993), 18 km^3 icebergs were calved into the fjord system. The Daugaard-Jensen glacier, draining into the Nordvestfjord, is one of the main contributors to iceberg production (*Cofaigh et al.*, 2001).
Nordvestfjord has a total length of 140 km and a width of about 5 km. Numerous smaller branches join this fjord which is separated from the Outer Scoresby Sund by a sill, shallowing the fjord floor to about 400 m (*Dowdeswell et al.*, 2016).

2.2 Sample and data collection

In summer 2016, a research cruise with the German research vessel *Maria S. Merian* (MSM56) with 22 international participants was conducted. Focus of this cruise was

the examination of the molecular ecological chemistry in Arctic fjords at different stages of deglaciation. For that, three fjords were examined: Kongsfjorden (Svalbard), Scoresby Sund (Greenland), and Arnarfjordur (Iceland). The present study is focussing only on samples from Scoresby Sund and its northernmost branch, the Nordvestfjord.
28 stations at the Greenland shelf, the Outer Scoresby Sund, and the Nordvestfjord were occupied in order to document the physical and biological conditions in Scoresby Sund, to assess the influence of glacial meltwater, and to estimate the biological and physical carbon pumps (Fig. 2.1).

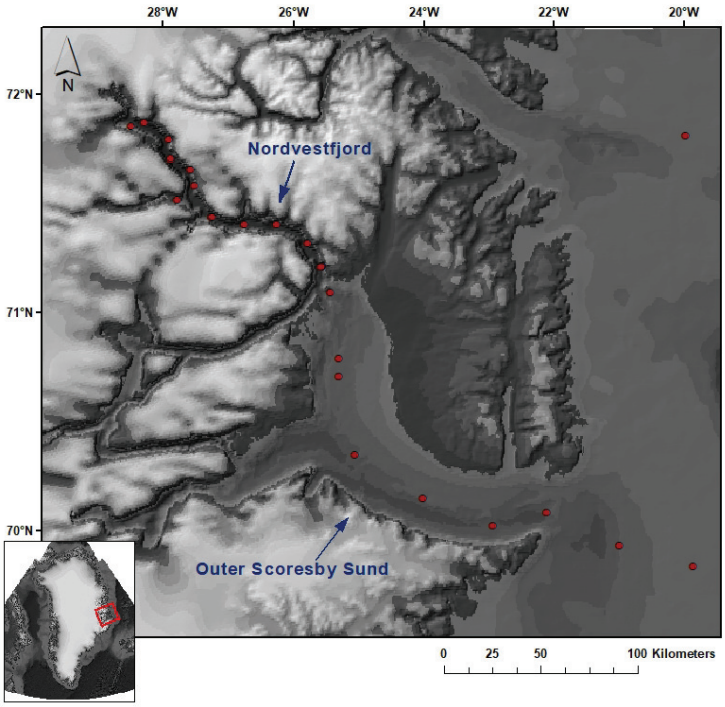

Figure 2.1: Map of Scoreby Sund including all stations occupied during the cruise MSM56 with RV *Maria S. Merian*. Arrows indicate the two main parts of Scoresby Sund: The Nordvestfjord and the Outer Scoresby Sund.

2.2.1 Water column sampling

At 25 stations, located at the shelf, in the Outer Scoresby Sund, and in the Nordvestfjord, conductivity-temperature-depth (CTD; SBE 9, Sea-Bird Scientific) as well as turbidity (ECO-NTU, WET Labs, Sea-Bird Scienfific), fluorescence (ECO-AFL/FL, WET Labs, Sea-Bird Scientific), PAR/irradiance (Biospherical instruments/LICOR),

and dissolved oxygen measurements (SBE 43, Sea-Bird Scientific) were collected using a SBE 11plus Deck Unit (Sea-Bird Scientific). The data were recorded during the down-cast, with a descent rate of 0.5 m s^{-1} to 100 m depth and of 1 m s^{-1} below 100 m.
The Deck Unit was additionally equipped with a 24-bottles rosette sampler with Niskin-type bottles. The bottles were closed during the up-cast at certain depths.
Dissolved oxygen samples were taken for sensor ground truthing at all stations. They were drawn into pre-calibrated biological demand flasks, treated with 1 ml $MnCl_2$ and 1 ml NaI/NaOH, and plugged. All samples were then measured on-board within 24 hours using Winkler titrations.
Water samples for later nutrient analyses were collected from almost all depths at each station in 50 ml PE bottles and stored frozen.
12 stations were sampled for DIC and TA following the instructions of the Guide to Best Practice for Ocean CO_2 measurements (*Dickson et al.*, 2007). Samples were drawn from the same respective Niskin bottle into ~300 ml borosilicate bottles. After collection, the samples were poisoned with 1 ml of 5% aqueous mercuric chloride ($HgCl_2$) solution to a final concentration of ~0.02%, leaving a headspace of 2 ml. The addition of $HgCl_2$ was aimed to hamper DIC concentration changes by biological activity. Subsequently, the bottles were sealed by greasing and additional fixation with adhesive tape, and stored cold and dark until further processing.
All samples for gas analyses (dissolved oxygen, DIC/TA) were taken first from the Niskin bottles to minimize the exchange with atmospheric gases on deck.

2.2.2 Surface pCO_2 record

A transportable Ferrybox system (Pocket Ferrybox, 4H JENA engineering, Jena, Germany) was installed to measure physical oceanographical parameters such as temperature, salinity, oxygen, and speed of sound, next to bio-optical parameters like chlorophyll and turbidity. Additionally, date, time, position, heading, and speed of the ship were recorded. The Ferrybox was supplied by water from the sea water pump system, originating from a water depth of 6.5 m and transported from the hydraulic extension unit to the laboratory via a centrifugal or membrane pump. The pCO_2 flow-through sensor (CONTROS HydroC CO_2 FT, Kongsberg) was connected to the continuous outflow of the Ferrybox because bubble entrainment and irregular flow occurred when it was directly connected to the seawater system of the ship. The sensor continuously recorded the partial pressure of CO_2, applying the infrared (IR) absorption spectrometry: Dissolved gases diffuse through a membrane and an internal gas circuit into a detector chamber, where the IR light intensity is dependent on the concentration of CO_2. For the output signal, the calibration coefficients stored in the firmware and data from additional sensors in the gas circuit were applied.

2.2.3 Data provided by other scientists

Several instrument applications and measurements were performed and provided by other scientists to add information for this thesis.

The CTD rosette was run by Anna Friedrichs and Kai Schwalfenberg from the *Institut der Biologie und Chemie des Meeres der Universität Oldenburg* (ICBM). Anna Friedrichs also processed and provided all physical oceanographic data obtained during the cruise.
Sampling and analysis of seawater samples for nutrient determination was performed by Claudia Burau and Jana Geuer from the research division Ecological Chemistry of the *Alfred-Wegener-Institut Helmholtz-Zentrum für Polar- und Meeresforschung* (AWI). The concentrations of nitrate, nitrite, phosphate, and silicate were measured using a spectrophotometric autoanalyser (Evolution III, Alliance instruments) with standard seawater methods (*Kattner and Becker*, 1991). In addition to samples from the rosette sampler, a couple of samples from surface meltwater runoff were analysed.
Drifting sediment traps were deployed at four stations (Fig. 2.1) at 100, 200, and 400 m depth for five to ten hours each. They were used to estimate, amongst others, the flux of particulate organic carbon (POC). The deployments as well as the analyses were conducted by Helga van der Jagt and Christian Konrad from the *Zentrum für Marine Umweltwissenschaften der Universität Bremen* (MARUM).
At 13 stations, Helga van der Jagt and Christian Konrad also deployed the in-situ particle camera. It has been self-constructed at MARUM and was equipped with an infrared camera (acE2040-25gc GigE camera, Basler) with backlight illumination (consisting of IR LEDs in an oil-filled pressure chamber and macrolon plates as diffusor panels) to investigate particle size and abundance in the water column. The pre-installed IR filter of the camera was removed. Every 25 seconds, one picture was made comprising a volume of 20.46 cm^3 of the surrounding water column. The exposure time comprised 1 ms while imaging an object pixel size of 22.56 µm. Picture analysis was performed after the cruise.

Table 2.1 summarizes the stations and equipment applied.

Table 2.1: Occupied stations and corresponding parameters in Scoresby Sund. The province defines the approximate location within the fjord. Sed. Trap = Sediment trap

Station	Province	CTD	DIC/TA	Nutrients	Camera	Sed. Trap
571	Greenland Shelf	x	-	x	-	-
572	Outer Scoresby Sund	x	x	x	x	x
574	Greenland Shelf	x	-	x	-	-
575	Greenland Shelf	x	x	x	-	-
576	Outer Scoresby Sund	x	-	x	-	-
577	Nordvestfjord	x	-	x	-	-
578	Nordvestfjord	x	-	x	-	-
579	Nordvestfjord	x	-	x	-	-
580	Nordvestfjord	x	x	x	x	-
582	Nordvestfjord	x	x	x	x	x
583	Nordvestfjord	x	-	x	-	-
584	Nordvestfjord	x	x	x	x	-
585	Nordvestfjord	x	-	x	-	-
586	Nordvestfjord	x	x	x	x	-
588	Nordvestfjord	x	-	x	-	-
590	Nordvestfjord	x	x	x	x	-
592	Nordvestfjord	x	x	x	x	x
593	Nordvestfjord	x	-	x	x	-
594	Nordvestfjord	x	-	x	-	-
595	Nordvestfjord	x	x	x	x	x
598	Outer Scoresby Sund	x	x	x	x	-
599	Outer Scoresby Sund	x	x	x	x	-
600	Outer Scoresby Sund	x	-	x	x	-
601	Outer Scoresby Sund	x	x	x	x	-
602	Outer Scoresby Sund	x	-	x	-	-

2.3 Sample and data analyses

2.3.1 DIC and TA

DIC and TA determination was performed using an analytical system consisting out of a VINDTA 3C (Versatile Instrument for the determination of Total inorganic carbon and titration Alkalinity, Marianda, Kiel, Germany) and a CO_2 coulometer (CM5015 Coulometer, UIC Inc., USA) (*Mintrop et al.*, 2000). Measuring temperatures were kept within a small range due to constant heating of the setup by a thermostat bath.

TA was determined with a Gran potentiometric titration (*Gran*, 1952) at 25°C by titrating 4.05 ml 1 N hydrochloric acid into an exactly known volume of sample. In

this mathematical approach, a fourth order curve fitting along a modified Gran plot (electrode potential vs. volume acid added) was performed. The titrant was prepared within a sodium chloride background to mimic the ionic strength of seawater (*Dickson et al.*, 2007). TA was corrected for nutrients (phosphate, silicate, borate) and density (using in-situ salinities and measurement temperature) by the Vindta software provided by the manufacturer of the instrument. Additionally, a volume correction was applied to account for the small dilution effect by the $HgCl_2$ addition (*Dickson et al.*, 2007).

DIC was measured performing a coulometric titration (*Johnson et al.*, 1993; *Dickson et al.*, 2007). An exactly known sample volume was acidified with 10% phosphoric acid to convert all carbonate and bicarbonate species into dissolved CO_2. Subsequently, a carrier gas (N_2) transported the CO_2 to the coulometric cell, where a chemical reaction changed the opacity of the cell solutions. As the required amount of charge needed to obtain the original opacity of the solutions is linear to the amount of dissolved CO_2, the concentration of carbonate species in a sample with known density could be back-calculated. To avoid bubble formation due to the low in-situ temperature during sampling, this measurement was performed at 10°C. Equally to TA, results were corrected for density and dilution. Besides, a correction for the introduction of additional DIC by the $HgCl_2$ solution was conducted (assuming a DIC concentration of 25 μmol kg^{-1}).

In the beginning of each day, three dummy measurements were performed in order to stabilize the Vindta system. TA as well as DIC were then calibrated against certified reference material (CRMs; provided by A.G. Dickson, Scripps Institution of Oceanography, USA, batches #102 and #161) and values adjusted according to the offsets for each measurement series (*Hartman et al.*, 2011). The correction factors ranged from 0.933 to 1.022 for TA and from 1.025 to 1.030 for DIC. Some samples from surface waters had very low salinities (~11). As no CRMs for low salinities (<~30) and low alkalinities (<~2000 μmol kg^{-1}) exist, *Bates et al.* (2014) suggest to assume that the quality assurance for low salinities still holds true, given that TA remains conservative relative to salinity and ionic strength and, thus, the ion balance of the alkalinity term is not altered significantly. Measurements had a precision of 1.8 μmol kg^{-1} for TA and 1.4 μmol kg^{-1} for DIC, respectively, based on several inter-bottle comparisons, each one drawn from the same respective Niskin bottle.

2.3.2 Surface pCO_2

Sensor output data were corrected according to the data processing sheet for CONTROS HydroC CO_2 distributed by Kongsberg using the software Matlab R2015a. The

sensor was pre-calibrated about three months before the cruise and post-calibrated about 14 months after the cruise by the manufacturer. Raw and reference signals recorded by the dual-beam NDIR detector together with a temperature-dependent factor taken from the pre-calibration sheet were used to compute the two-beam signal.

For the baseline drift correction, zeroing data (regular zeroing intervals for 5 to 10 minutes every 12 hours) were extracted and the mean signal of each zeroing interval was determined. The first 30 seconds of each interval were discarded as they still contain the signal drop from the ambient to zero CO_2 concentration. Subsequently, zeroing intervals before the sensor deployment as well as zeroing intervals with a standard deviation > 2 were excluded from further processing. Between each of the remaining zeroing signals, a linear interpolation was performed, and the drift-corrected signal was determined using these linear fits, the two-beam signal, and a NDIR-specific scale factor obtained from the pre-calibration sheet.

To account for the sensor's concentration dependent characteristics, a span drift correction was performed. This correction aims to transform the polynomial of the pre-calibration to the polynomial of the post-calibration using the calibration coefficients from each, the pre- and the post-calibration sheet. By applying the formula given in the Kongsberg processing sheet, the calibration factors become dependent on the linearly interpolated zero signals. In this step, the first time stamp after the pre-calibration and the last time stamp before the post-calibration were considered for the calculation, mirroring the total runtime of the sensor.

Subsequently, pCO_2 in parts per million (ppm) was computed using the calibration factors obtained during the span drift correction and the baseline drift-corrected signal calculated during the first correction step. For reference gas temperature and cell pressure, standard values from the pre-calibration sheet were used. Additionally, gas temperature and cell pressure during the deployment, given by the sensor's output, had to be applied in this calculation. pCO_2 in µatm could be calculated by considering the pressure behind the membrane, which was also recorded by the sensor.

The data were then cleaned from zeroing intervals, outliers, and non-cruise data. Besides, the first five measurements after each zeroing interval were excluded, as they showed a lower signal then expected based on the surrounding signals. It was assumed that the signal was still recovering from the zero measurement and did not record the ambient CO_2 concentration, even if this was not displayed in the output data of the sensor.

Finally, pCO_2 was corrected for the in-situ surface water temperature according to *Takahashi et al.* (2009):

$$pCO_2(T_{in\text{-}situ}) = pCO_2(T_{meas}) \cdot exp[0.0433 \cdot (T_{in\text{-}situ} - T_{meas}) - 4.35 \cdot 10^{-5} \cdot (T^2_{in\text{-}situ} - T^2_{meas})], \quad (2.1)$$

where $T_{in\text{-}situ}$ is the in-situ temperature of the surface water and T_{meas} is the temperature where the actual partial pressure of CO_2 is measured. As the sensor was connected to the continuous outflow of the Ferrybox, water temperature recorded by the Ferrybox could be taken as measuring temperature. The in-situ temperature was measured along the whole cruise track by sensors at the ship's seawater intake and recorded within the data management system DAVIS-SHIP (DSHIP, GEOMAR Helmholtz-Zentrum für Ozeanforschung Kiel) installed on RV *Maria S. Merian*. Datasets could be matched using the according time stamps, accounting for about 10 minutes delivery time through the 40 m long water line between intake and sensor. Likewise, the corrected data were aligned with the coordinates given by DSHIP to display the geo-referenced surface pCO_2. Each alignment was performed by rounding the exact measuring time of the sensor to one measurement per minute.

2.3.3 In-situ particle camera

In-situ particle camera pictures were analysed using the software Matlab R2015a. Basic routines were provided by Morten Iversen and Christian Konrad (MARUM), but were edited and improved for the purpose of the present study. Particle abundance and size were recognized by the software after converting the pictures into binary files and correcting them for background disturbances, such as shadows from illumination artefacts and spots on the camera lens. Particles were then binned into 20 size classes (d), ranging from 20 to 3415.03 µm. Each picture was concatenated to its respective in-situ depth. Knowing the volume of the water cell pictured by the camera, the number of particles per litre and size class could be calculated (ΔC). To account for statistical relevance, especially for the barely occurring large particles, always 10 consecutive pictures were summarized. For calculating the particle size spectra n, the number of particles per litre in a given size class was divided by the size difference between the concomitant size classes, as described by *Iversen et al.* (2010):

$$n = \Delta C / \Delta d. \quad (2.2)$$

Particle volume spectra nVd were calculated following the procedure of *Petrik et al.*

(2013):

$$nVd = n \cdot (\pi/6) \cdot d_i^4 \tag{2.3}$$

where d_i is the median of the ith bin size range. This gives the total volume within a given size range, assuming spherical particles.

The calculation of the total POC flux needs further assumptions. The aim was to fit the flux estimation to given POC flux values at certain depths, which were obtained by the sediment trap deployments. In general, the POC flux determination is comparable to the method used by *Iversen et al.* (2010). They assume that the total POC flux F can be obtained from an integration of the mass flux spectra of all particle sizes:

$$F = \int_0^\infty n(d)m(d)w(d)d(d) \tag{2.4}$$

where *m(d)* is the mass of a particle with the size d and *w(d)* is its respective sinking velocity. The particle size spectra n and the particle diameter d are known, whereas m and w have to be determined. Both parameters are assumed to follow power functions. Thus, they can be combined to:

$$mw = \mathrm{A} \cdot d^{\mathrm{b}} \tag{2.5}$$

By combining this function with the respective other parameters, the flux could be determined depending on A and b. Each camera profile was assigned to a drifting sediment trap nearby, resulting in one to three profiles per trap.
Now the known POC flux from the associated sediment trap, F_{trap}, at a certain depth could be applied. The assumption was made that F_{trap} holds true for a depth interval of 20 m. For example, if the sediment trap had been deployed at 200 m, the flux was expanded to an interval of 190 to 210 m. For this interval, the according F was calculated, which is still dependent on A and b. Note that the integration in equation 2.4 was only used for particles within the above-mentioned 20 size classes, and not for sizes from 0 to ∞. Subsequently, the best fit between both fluxes could be determined, resulting in values for A and b. To achieve this fit, the Matlab function *fminsearch* was applied. Now knowing A and b, the total POC flux for the whole depth covered by camera pictures could be generated.

2.4 Data compilation and visualisation

2.4.1 Determination of the net community production

The NCP within one year is displayed in the seasonal consumption or production of the photosynthetic reaction products (*Mathis et al.*, 2010), like dissolved inorganic carbon, phosphate, and nitrate, and can therefore be estimated by determining the drawdown of these inorganic components in the surface ocean (*Ulfsbo et al.*, 2014). Usually, the change in the budgets of these parameters is determined by measurements before and after the main growing season. The difference between both data sets is then computed within the mixed layer, which is mostly assumed to be 30 m (*Bates et al.*, 2005; *Mathis et al.*, 2009, 2010; *Bates et al.*, 2014; *Munro et al.*, 2015; *Reisdorph and Mathis*, 2015).

Often, however, it is not possible to visit a sampling site twice a year, especially in remote areas such as the Arctic Ocean. In this case, different approaches have been used. For example, *Anderson et al.* (2003) assumed a conservative behaviour of the inorganic components and determined their concentrations in the source waters of the research area, considering these as initial concentrations. *Lee* (2001) used a modelling approach to estimate NCP on a global scale.

The third way to determine NCP using only one set of measurements per sampling site is applied here. It assumes a remnant winter water layer which still contains the inorganic components in unchanged concentrations, representing the initial budget. This can then be compared to the actual concentrations within the water layer above (*Jennings Jr et al.*, 1984; *Hansell and Carlson*, 1998; *Hoppema et al.*, 2000, 2007; *Ulfsbo et al.*, 2014). Depletions of DIC, nitrate/nitrite, and phosphate were computed.
The remnant winter water can be identified using CTD profiles and is defined as temperature minimum below the halocline with a weak salinity gradient (*Rudels et al.*, 1996; *Ulfsbo et al.*, 2014). The temperature should be close to the freezing point, and as the water layer above is relatively warm and fresh, this winter water is kept out of contact with the atmosphere (*Hoppema et al.*, 2000, 2007).

An obvious winter water layer as described above could only be defined at the Greenland shelf stations. The fjord stations showed a clear temperature minimum, whereas the salinity increased exponentially with depth. Several processes could have led to internal mixing resulting in a less distinct salinity stratification. First, tides could have moved the water within the fjord so that the stratification between

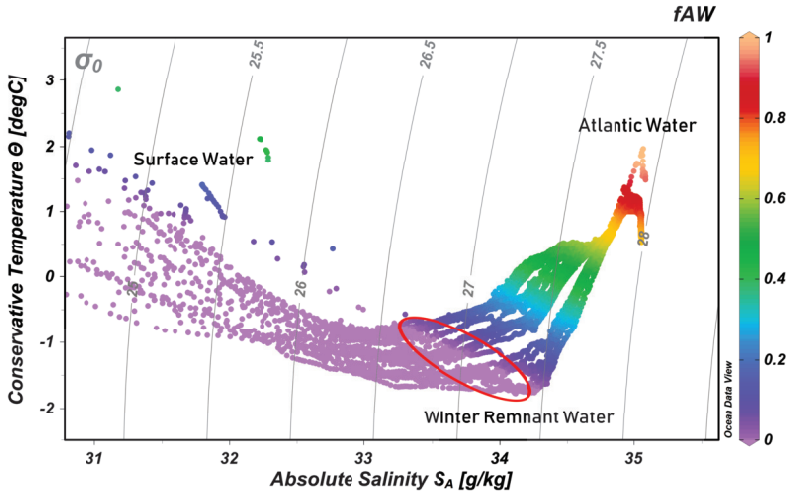

Figure 2.2: T/S plot of the waters in Scoresby Sund, with color bar showing the fraction of Atlantic Water (fAW). The red circle indicates waters at the depths of the temperature minima.

the water masses could have been disturbed. Second, marine-terminating glaciers, which are also present in Scoresby Sund, could have released melting plumes from subglacial runoff with a lower density compared to the surrounding water. If these plumes ascent, they lead to mixing of the water (e.g. reviewed by *Straneo and Cenedese*, 2015). Third, velocity pulses originating from the shelf as a result of storm events could have led to internal mixing of the fjord waters (*Jackson et al.*, 2014; *Jackson and Straneo*, 2016). Whatever process was responsible for internal mixing of water masses within the fjord, it could have resulted in vertical advection of inorganic components, replenishing the surface waters with components that were previously used up by primary producers and therefore biasing the NCP calculation which is based on drawdown by primary production of these components. Especially Atlantic Water coming into the fjord below the Polar Water at the surface is believed to hold a higher concentration of nutrients than the neighbouring water masses. Therefore, an endmember analysis was performed to evaluate the share of Atlantic Waters at the depth of the temperature minimum and above. Three endmembers could be identified: Atlantic Water, Surface Water, and Winter Remnant Water. Following the T/S plot (Fig. 2.2), the Atlantic Waters made up only a negligible fraction of the waters at the depth of the temperature minima and above. Thus, vertical mixing seems to be an important process at depth, but not at the surface where NCP takes place.

Looking at the current pattern along the eastern coast of Greenland, it seems that the inshore branch of the East Greenland Current, transporting Polar and Atlantic

Water from north to south on the continental shelf (*Bacon et al.*, 2002; *Håvik et al.*, 2017), feeds the Scoresby Sund. Assuming that it takes approximately one season for the fjord water to be replaced, the mean DIC and nutrient concentrations of the temperature minima at the shelf stations was taken as initial concentrations for the whole fjord. The depth of the mixed layer during winter is assumed to be shown in the temperature minimum of each station.
By using these values, the following equation was applied (modified after *Ulfsbo et al.*, 2014):

$$NCP_x\,[mmol\,C\,m^{-2}\,period^{-1}] = \int_0^{T_{min}} (X_{initial} - X_{measured})dz \cdot R_{C/X}, \tag{2.6}$$

where X represents the concentration of the relevant components, either taken from the shelf stations (initial), or measured at each sampling depth. $R_{C/X}$ is the nutrient stoichiometric ratio which is necessary to convert nutrient units to carbon units. In this study, the Redfield ratio (106 Mol C : 16 Mol N : 1 Mol C) was used. The integration was performed by linear interpolations between nearest sampling depths.
Prior to this, concentrations were normalized to a constant salinity of 34.5 to exclude the dilution effects by sea-ice melt, evaporation, and precipitation:

$$X_{initial\,or\,measured} = X_{S\,in\text{-}situ} \cdot (34.5/S_{in\text{-}situ}). \tag{2.7}$$

$S_{in\text{-}situ}$ is the salinity at sampling depth and $X_{S\,in\text{-}situ}$ the uncorrected concentration. For phosphate and nitrate/nitrite, a zero freshwater endmember could be assumed, as a non-zero freshwater endmember would change the resulting NCP_{PorN} only slightly. For DIC, however, a different correction had to be applied, as the freshwater coming into the fjord seems to contain relatively high DIC concentrations. A linear regression between DIC concentrations and salinities of samples with salinities of more than 30 (surface samples with lower salinities were assumed to be changed by biological activity) resulted in a considerable DIC concentration of 423 µmol kg^{-1} at a salinity of zero. Thus, the normalization was performed using the approach of *Friis et al.* (2003):

$$X_{initial\,or\,measured} = ((X_{S\,in\text{-}situ} - X_{S=0})/S_{in\text{-}situ}) \cdot 34.5 + X_{S=0}, \tag{2.8}$$

where $X_{S=0}$ is the DIC concentration at a salinity of 0.

The calculated NCP now represents the time-integrated changes of the summer and winter surface layers from the end of the winter period to the time of sampling (*Ulfsbo et al.*, 2014).
Using Landsat satellite images (USGS, EarthExplorer, Landsat 8 OLI/TIRS C1 Level-

1), the approximate time of ice breakup could be evaluated. Together with the sampling date and the assumption that primary production approximately starts with ice breakup, NCP per day was calculated.

2.4.2 Determination of the remineralisation and sedimentation to the sea floor

To obtain an impression how much of the NCP at the surface is remineralised within the upper 200 m of the water column, the decrease in POC flux from the maximum POC flux within the upper 100 m of the water column down to 200 m was determined. The mean flux within a depth interval of 20 m around each afore-mentioned depth was calculated to exclude the over-representation of single measurement points.

To determine the sedimentation of particulate organic carbon on the ocean floor, a widely used power function approximation describing the decrease of POC flux with depth, originally proposed by *Martin et al.* (1987), was applied:

$$F(z) = F(z_0) \cdot (z/z_0)^{-b}, \tag{2.9}$$

where F are the POC fluxes at the respective depths, z_0 and z, and b is the remineralisation exponent. This exponent can also be considered as efficiency of which the carbon exported from the upper ocean, i.e. $F(z_0)$, decreases with depth (*Guidi et al.*, 2015). Most applications of this formula are based on data from open ocean sediment trap deployments (*Martin et al.*, 1987; *Francois et al.*, 2002; *Boyd and Trull*, 2007; *Belcher et al.*, 2016), thus, the application on fjord carbon fluxes with intense lateral advection has to be considered with caution. It is, however, frequently used in modelling approaches (*Boyd and Trull*, 2007), and b has a high regional variability (*Francois et al.*, 2002; *Guidi et al.*, 2015) which needs to be considered in estimations of the global carbon sequestration. Regarding the consistency of global remineralisation calculations, it seems to be reasonable to apply the same formula in the present work. Additionally, the camera profiles only cover about one third of the whole depth at the respective stations, which makes an interpolation necessary.

For determining b for each station, the power function was fitted to the POC flux profiles obtained from the particle camera pictures. The depth of the maximum POC flux within the upper 100 m was taken as reference depth z_0. To prevent the overestimation of the flux at depth due to resuspension from the bottom, the maximum profile depth minus 50 m was taken as z. In order to smooth out single peaks in POC flux, an interval of 20 m around each depth, z_0 and z, was considered to calculate

the mean POC flux at the respective depth. High b values indicate high degradation, while negative b values show strong attenuation or initially increasing POC fluxes with depth.
The b values obtained from this calculation could now be used to identify the portion of the NCP which might reach the sea floor. For this, the depths z_0 of the maximum POC fluxes were kept, but the fluxes $F(z_0)$ were replaced by the different NCPs in g m^{-2} d^{-1}. When applying the bottom depths as z, the fluxes at the seafloor could be calculated.

2.4.3 Visualisation

All maps were created using ArcGIS Desktop 10.5.1 and are displayed in WGS84 UTM27N (UTM23N for the overview map of Greenland). The positions of strong meltwater discharge and marine-terminating glaciers were obtained by visual inspection of Landsat satellite images (USGS, EarthExplorer, Landsat 8 OLI/TIRS C1 Level-1), recorded during the time of the expedition.
Physical, chemical, and biological parameters were visualised using section plots of the Ocean Data View 4 software (ODV). In most cases, Data-Interpolating Variational Analysis (DIVA) was applied. For sections with less data points, like POC flux and TA/DIC concentrations, plots were created using a weighted-average interpolation method (both computed by ODV).
Matlab R2015a was used for the analyses and visualisations of the linear regressions. The overview figure was created with Inkscape 0.91.

2.4.4 Uncertainties

Several uncertainties may come along with the laboratory and mathematical analyses, which might have a slight effect on the results and should be kept in mind during data interpretation.

The sample analyses regarding DIC and TA were performed with the highest accuracy possible. Nevertheless, the volume of the pipettes could have changed somewhat because of grease which was transported into the system by the sample (*Johnson et al.*, 1993). To minimize this error, pipettes and tubes were rinsed daily with deionized water.
TA was only corrected for phosphate, silicate, and borate, according to the most relevant nutrients being responsible for changes of TA in open ocean waters, which is the usual procedure. However, nutrient compositions and concentrations might be different in fjord waters.

Pictures of the particle camera were analysed using minimum and maximum numbers of pixel comprising one particle. Hence, the size range did not cover all particles in the ocean. Different numbers and sizes of the size classes, or bins, do not change the results, because the particle size spectra and particle volume spectra stay unaffected (*Jackson and Burd*, 2015). The width of the size range, however, can indeed influence the flux estimate (*Guidi et al.*, 2008). Flux estimates therefore depend on the camera, quality of the pictures, image analysing tool, and size range width chosen.

When calculating NCP in the above-mentioned manner, the following assumptions had to be made: little vertical or lateral mixing, which could add reactants from other areas; homogeneity of the water column during winter; depletion of nutrients (and other reactants) within a realistic time frame; and a negligible winter drawndown (*Jennings Jr et al.*, 1984; *Hoppema et al.*, 2007). Using DIC for the NCP determination, underestimation can occur when sea-ice melt contribution and air-sea gas exchange is not considered (*Mathis et al.*, 2010; *Bates et al.*, 2014; *Ulfsbo et al.*, 2014). When accounting for the budget change in nutrient concentrations, underestimations can result from the preferential remineralisation of a certain nutrient compared to others (*Jennings Jr et al.*, 1984; *Munro et al.*, 2015). Also the stoichiometry of the nutrient uptake by plankton can be variable (*Jennings Jr et al.*, 1984; *Mathis et al.*, 2010). It is therefore suggested to put more focus on individual plankton functional types when considering the nutrient stoichiometric ratios (*Silyakova et al.*, 2013).

Strong lateral advection between 100 m and 200 m depth could have biased the calculation of remineralisation and sedimentation estimates, as im- and export can mask the effect of the POC flux decrease with depth either by elevating or by reducing the particle number at depth. Also stratification of water masses with different POC content can lead to wrong assumptions of the vertical decrease in POC concentration.

Chapter 3

Results

3.1 Hydrography and bathymetry

Scoresby Sund is influenced by several marine-terminating glaciers as well as strong meltwater outflows from land-terminating glaciers. The most prominent marine-terminating glacier is the Daugaard-Jensen glacier at the fjord head with a width of about 22 km. The closest station occupied in this study has a distance of about 12 km to the glacier's front. Because smaller glaciers are not well documented, they were identified using satellite images from the time of the cruise. Only easily visible marine-terminating glaciers and large meltwater rivers are taken into account, whereas some smaller glacier arms and meltwater outflows could not clearly be seen and are therefore ignored. Three glaciers draining into Nordvestfjord and two glaciers draining into the Outer Scoresby Sund were counted, with front widths of 1 to 11 km. The depths of the glacier fronts are not known. In total, nine large meltwater rivers could be identified, seven of them in Nordvestfjord and two in the Outer Scoresby Sund (Fig. 3.2).

Pathways and types of meltwaters in the GrIS can be subdivided by their origin into three groups: supraglacial, englacial, and subglacial meltwater (*Nienow et al.*, 2017). Since surface (supraglacial) meltwater can also enter the englacial and subglacial drainage systems and be discharged into the fjord at depth, this so-called subglacial discharge (*Straneo*, 2017) and the submarine melt (meltwater below sea level) will not be distinguished further in this study, and both terms will be used interchangeably. However, it has to be mentioned that while subglacial discharge develops a buoyancy forcing at a fixed depth, submarine melting and, thus, its buoyancy forcing, occurs alongside the whole glacier front that is immersed in water (reviewed by *Straneo and Cenedese*, 2015).

According to visible observations, icebergs from calving glaciers were present all over the fjord, considerably more, however, in Nordvestfjord and with increasing density towards the fjord head.

Similar to observations of *Rysgaard et al.* (2003) in the more northerly fjord Young Sound, a large opening in the ice cover at the fjord mouth could be observed on satellite images, which persisted during the whole winter. In Young Sound, these openings were attributed to high current velocities from tidal forces. Since the same coastal currents affect Scoresby Sund, it is probable that the ice cover opening at Scoresby Sund's fjord entrance was developing similarly.

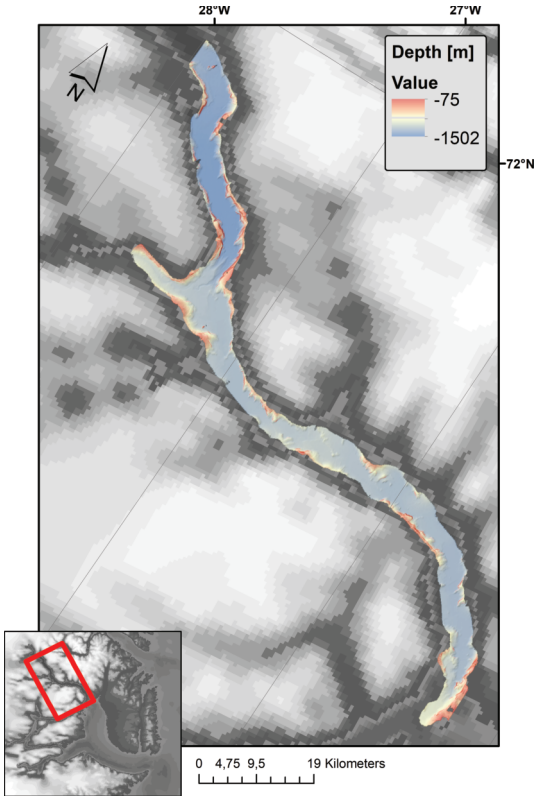

Figure 3.1: Bathymetry in Nordvestfjord, obtained from the ship's side scan sonar system.

Three water masses are feeding the fjord: Polar Water, Atlantic Water, and Greenland Sea Deep Water. Atlantic Water (Temperature > 1°C and Salinity > 34.65) enters the fjord at a depth of 250 to 400 m, below a layer of light Polar Water. The Atlantic Water fills the deep basins of Nordvestfjord. At the bottom, Greenland Sea Deep Water (Temperature < 1°C and Salinity > 34.85) is transported into the Outer Scoresby

Sund, but stays there due to a sill with a depth of about 350 m, which separates the Outer Scoresby Sund and Nordvestfjord. In Nordvestfjord, heat and freshwater are mixed downwards, establishing a layer of Modified Polar Water at the depth of the Polar Water. At the surface, a thin layer of glacial melt (Salinity < 33) covers the whole fjord in the upper 5 to 10 m.

While the Outer Scoresby Sund has a rather uniform bottom topography with a depth of about 600 m and decreasing slightly towards the shelf, Nordvestfjord is characterised by steep sills and basins between 500 and 1500 m (Fig. 3.1). The afore-mentioned stretched sill extends at the inner part of the Outer Scoresby Sund, separating it from Nordvestfjord by water depths of about 350 m.

In the further analysis, the whole fjord system is first considered with regard to the distribution of surface pCO_2 and normalised TA/DIC. After that, Scoresby Sund is subdivided into three regional domains based on the different regimes created by hydrology and bathymetry within the fjord: Nordvestfjord, the sill between Nordvestfjord and Outer Scoresby Sund, and the Outer Scoresby Sund together with the shelf. A summary of mean production, POC flux, and remineralisation values for Nordvestfjord, the Outer Scoresby Sund, and the Greenland Shelf can be found in Table 3.1. Only for the description of smaller scaled features in the fjord, production and remineralisation rates at single stations are taken into account. Furthermore, as NCP based on DIC depletion is significantly different from those obtained from nutrient concentrations, it is considered separately.

3.2 Surface pCO_2

Most surface areas in Scoresby Sund are supersaturated with regard to pCO_2, having pressure values of 400 to 490 µatm (Fig. 3.2). The largest variabilities can be found in regions influenced by meltwater discharge at the surface. At some spots, pCO_2 can even reach 680 µatm, whereas others are undersaturated with pressures of 380 µatm. Most extreme values are close to the Daugaard-Jensen glacier and at a spot in Nordvestfjord. They are described in more detail in the Sections 3.4.1 and 3.4.2.

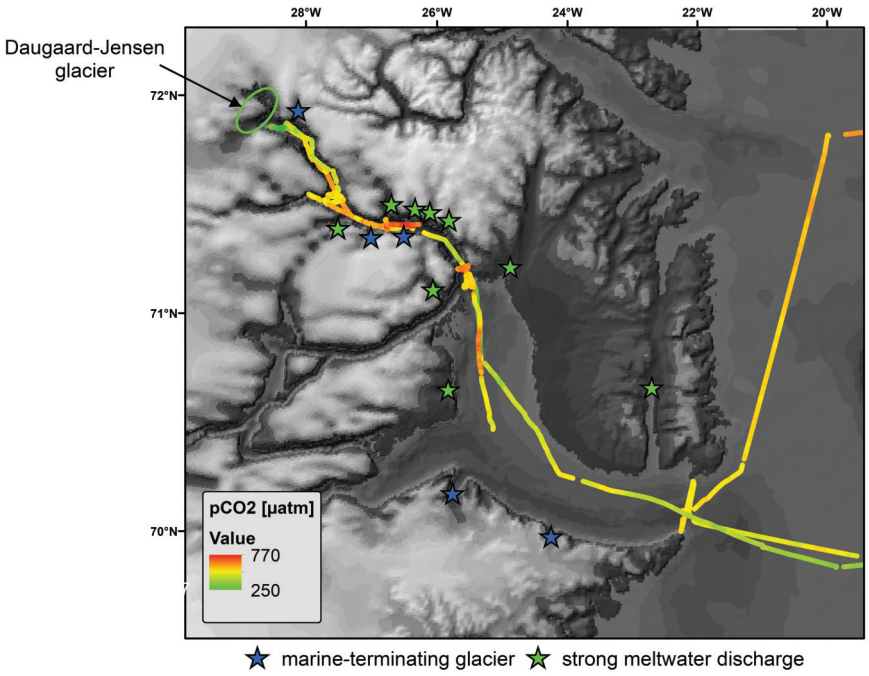

Figure 3.2: Surface pCO_2 concentration along the cruise track in Scoresby Sund. The position of the Daugaard-Jensen glacier as well as smaller marine-terminating glaciers and surface meltwater discharge are indicated on the map.

3.3 Normalised TA and DIC

DIC and TA do highly correlate with salinity, with R^2 of 0.906 and 0.942, respectively (Fig. A.1). To highlight processes other than dilution, both parameters were normalised to a constant salinity. Values deviating from a constant concentration then mirror processes like primary production, microbial processes, and carbonate mineral dynamics. While DIC can still be influenced by a number of factors, TA is traditionally seen as a conservative parameter. Any non-conservative behaviour of TA is attributed to mainly three processes: the accumulation of organic carbon, denitrification, and carbonate mineral precipitation and dissolution (*Cross et al.*, 2013). Hence, to highlight changes in the carbonate mineral budget, TA would have to be corrected additionally for the other two processes. However, since their influence on non-conservative TA behaviour is minor (*Cross et al.*, 2013), these corrections are ignored in this study.

Fig. 3.3 shows the normalised TA and DIC concentrations related to the sample salinities. Low salinities belong to the surface samples in Nordvestfjord.

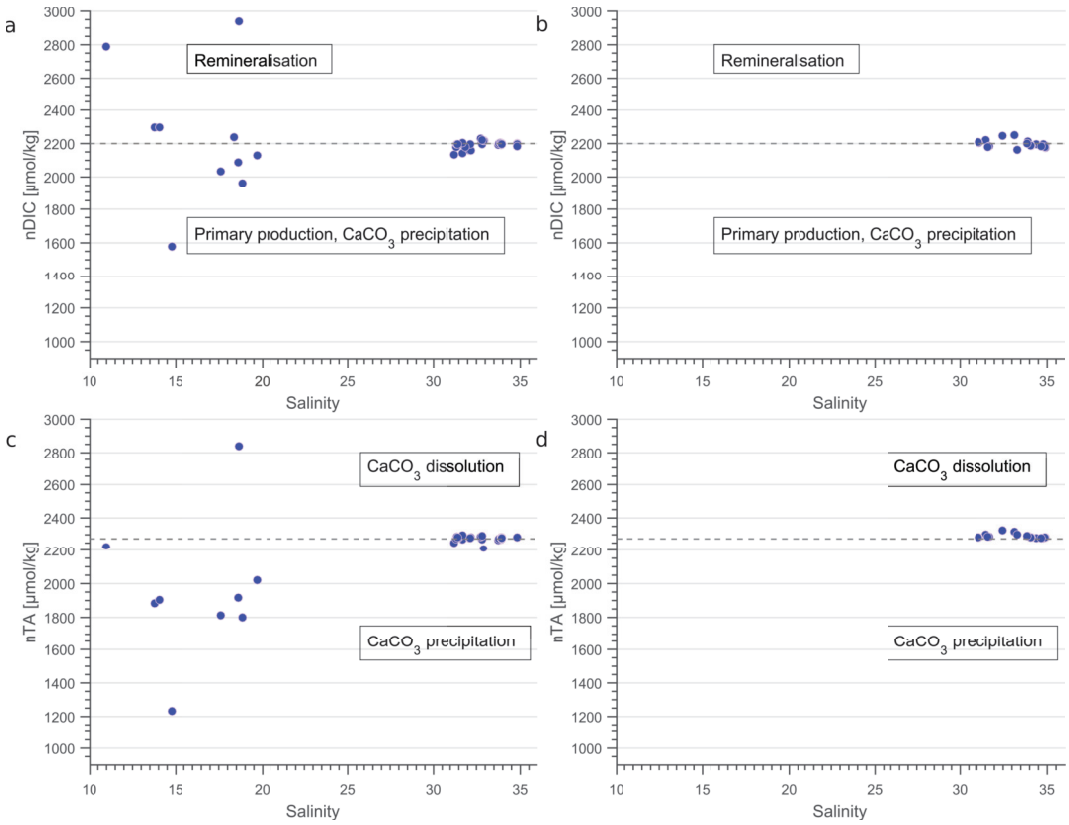

Figure 3.3: nDIC and nTA normalised to a constant salinity of 34.5 in relationship to sample salinity of all samples in Nordvestfjord (a,c), and Outer Scoresby Sund with the Greenland shelf (b,d). Non-zero freshwater endmembers were assumed for normalisation (*Friis et al.*, 2003). Dashed horizontal grey lines show the approximate mean of samples with a similar nDIC and nTA, respectively, to highlight deviations indicating biological and/or carbonate dynamics.

The normalisation of DIC reveals that primary production as well as remineralisation takes place in the surface layer of Nordvestfjord (Fig. 3.3a), while this cannot be seen in the samples of the Outer Scoresby Sund and the shelf (Fig. 3.3b). Likewise, nTA concentrations of the Outer Scoresby Sund and the shelf do not differ at different depths (Fig. 3.3d). In Nordvestfjord, mainly carbonate mineral precipitation takes place in the surface low-salinity layer (Fig. 3.3c). One surface sample, however, indicates the dissolution of carbonate minerals. This sample can be attributed to the mid-Nordvestfjord pattern, which is described in more detail later on.

3.4 Nordvestfjord

Bathymetry measurements in Nordvestfjord show that the maximum depth in this fjord arm is about 1500 m with steep slopes towards the coast (Fig. 3.1). The inner

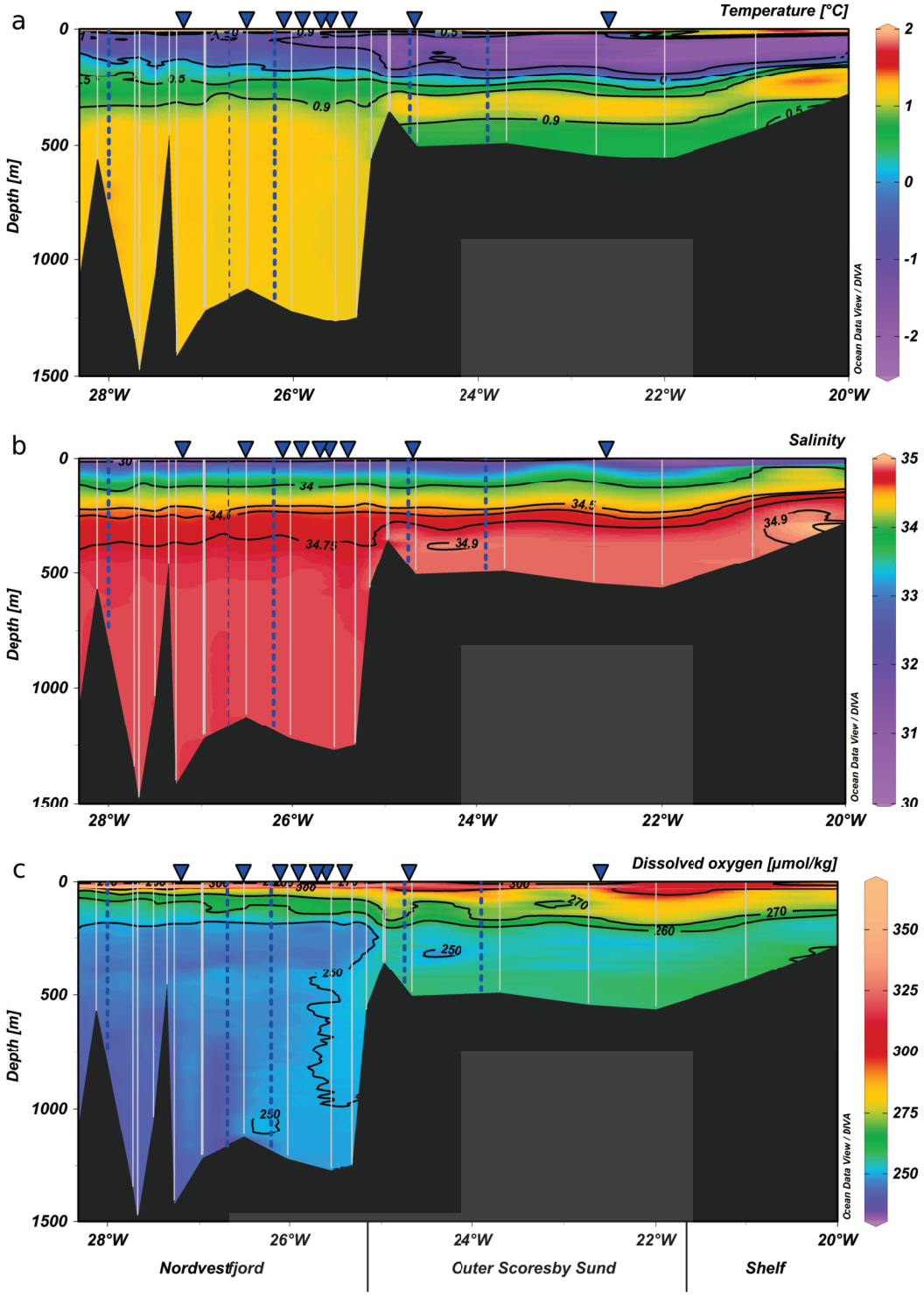

Figure 3.4: (a) Temperature, (b) salinity, and (c) dissolved oxygen along the transect from the fjord head (left) to the fjord mouth (right). Stations and sampling depths are indicated by white vertical lines. Blue vertical lines indicate the positions of marine-terminating glaciers, blue inverse triangles show the positions of surface meltwater inflow. Note that on the very left side (fjord head), the Daugaard-Jensen glacier calves into the fjord.

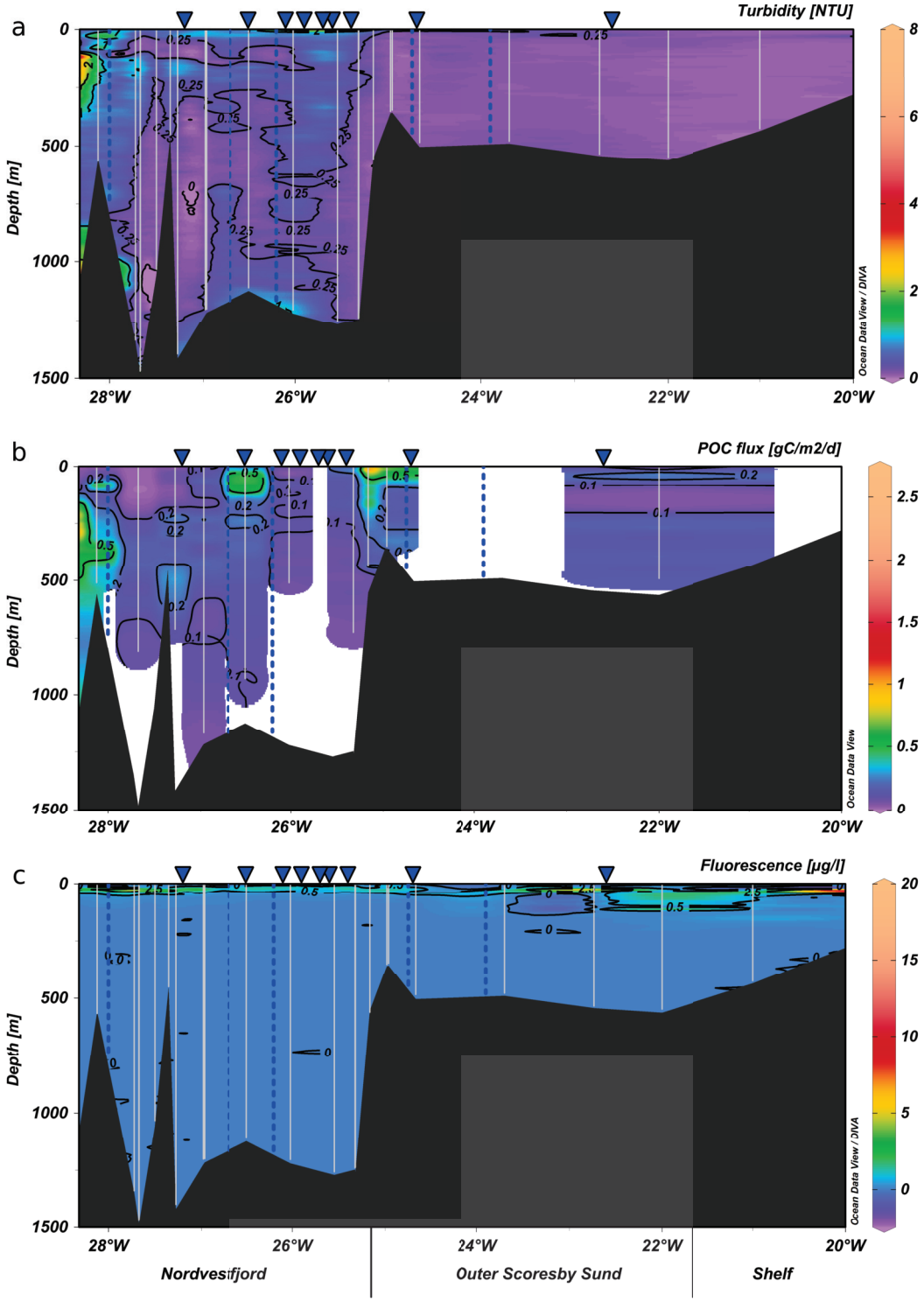

Figure 3.5: (a) Turbidity, (b) flux of particulate organic carbon (POC), and (c) fluorescence along the transect from the fjord head (left) to the fjord mouth (right). Labelling is similar to Fig. 3.4.

part of Nordvestfjord is the deepest, while the fjord rapidly becomes shallower towards the entrance to Outer Scoresby Sund.

Section plots covering the whole depth range are shown in the present chapter, while in the appendix, the same plots covering only the upper 500 m are presented for a better resolution of the surface layer (figure numbers starting with A).
Surface waters are heated by solar radiation to temperatures of up to 12.5°C, but are close to the freezing point just below this warm 5 to 10 m thick layer (Fig. A.2a). At depth, temperature is slightly increasing to 1 to 2°C (Fig. 3.4a). A fresh water layer with salinities down to 5 (Fig. A.2b) coincides with the heated surface. Below that, salinities strongly increase towards the bottom. The deep basin of Nordvestfjord is filled with waters having a salinity of about 34.9 (Fig. 3.4b).
Warmer and less saline water at greater depths compared to the Outer Scoresby Sund indicates a strong vertical mixing of the water column (Fig. 3.4a and 3.4b). Oxygen is depleted in deeper water layers, whereas the surface is highly ventilated (Fig. 3.4c). This can also be seen in the apparent oxygen utilisation rate (AOU, Fig. 3.7c and A.5c), which has been calculated by default from the software ODV. Turbidity (Fig. 3.5a and A.3a) is elevated at several locations within the whole water column with highest values next to Daugaard-Jensen glacier at 100 to 200 m depth (4 – 8 NTU) and at the surface between 25 and 26°W (2 – 4 NTU). A high fluorescence layer with up to 5 μmol l^{-1} could be observed at about 25 m depth (Fig. 3.5c and A.3c). Nutrients (Fig. 3.6 and A.4) are depleted at the surface down to 0 to 0.1 μmol l^{-1}, but patchily elevated within the remaining water column (highest values: 12 μmol l^{-1} nitrate+nitrite, 0.8 μmol l^{-1} phosphate, and 7 μmol l^{-1} silicate). Only silicate has a high concentration at the surface (up to 6 μmol l^{-1}) where lots of meltwater rivers drain into the fjord (25 – 26°W) (Fig. 3.6c and A.4c). Fig. 3.7a,b shows the DIC and TA concentrations without salinity normalisation. In most parts of the fjord, concentrations strictly follow the salinity distributions. Patches deviating from this relationship can barely be identified.

NCP in Nordvestfjord is 30.9 mmol C m^{-2} d^{-1} based on phosphate depletion and 34.7 mmol C m^{-2} d^{-1} based on nitrate+nitrite depletion, respectively, accounting for the number of days of open water since winter. An estimated net community production of -0.3 mmol C m^{-2} d^{-1} using the depletion of dissolved inorganic carbon shows that DIC must have been introduced to the system at the surface (Table 3.1).

POC flux is elevated at patches next to Daugaard-Jensen glacier and at some locations within the fjord (Fig. 3.5b), with about 0.5 to 2 g C m^{-2} d^{-1}. The particle size spectra, which were calculated during the analysis of the particle camera pictures, show that particles are larger where the POC flux is high, and become smaller with

decreasing POC flux.

The NCP is remineralised by only 12 to 20% within the upper 200 m of the water column when considering the production calculated with nutrient depletions (Table 3.1). However, im- and export of particulate material by lateral advection have to be kept in mind. A fraction larger than the NCP (1.03 and 0.95 g C m^{-2} d^{-1}, respectively) is sedimenting onto the sea floor, and the *b* value is relatively low with 0.11.

Within Nordvestfjord, two regions can be observed that stick out from the general pattern. The first region is the area close to the Daugaard-Jensen glacier. The second region is an area between 26 and 27°W, where all parameters are distributed differently than in the adjacent areas.

Table 3.1: Production, carbon flux, and remineralisation in Nordvestfjord, Outer Scoresby Sund (Outer Sc. Sund), and Greenland Shelf. NCP_{nuts} is the determined based on nitrate+nitrite as well as phosphate deficits, NCP_{DIC} based on DIC depletion. $Remineralisation_{200}$ refers to the remineralisation of the corresponding NCP_{nuts} within the upper 200 m, POC_{bottom} is the POC flux that reaches the bottom, computed using the *b* value. All values were averaged for the acccording region. For the shelf, remineralisation values are not available.

	Nordvestfjord	Outer Sc. Sund	Greenland Shelf
NCP_{nuts} [mmol C m^{-2} d^{-1}]	30.9 - 34.7	43.2 - 67.3	52.0 - 61.9
NCP_{DIC} [mmol C m^{-2} d^{-1}]	-0.3	-36.1	-124.3
$Remineralisation_{200}$ [%]	12 - 20	73 - 91	-
b value	0.11	0.34	-
POC_{bottom} [g C m^{-2} d^{-1}]	0.9 - 1.0	0.2	-

3.4.1 Daugaard-Jensen glacier

With up to 258 µatm, the lowest surface pCO_2 values are observed in direct vicinity to the glacier. Salinity drops by 0.1 to 0.2 units at a depth of 200 to 250 m towards the surface. Slightly higher up in the water column at a depth of 100 to 200 m, nutrient concentrations are reduced by half compared to values in the surrounding waters (Fig. 3.6 and A.4). At the same depth, turbidity is high with $4 - 8$ NTU, whereas elevated POC flux values (up to 1 g C m^{-2} d^{-1}) can be observed at 250 to 400 m depth (Fig. 3.5a,b and A.3a,b). Without a distinct increase in the NCP at the surface, the sedimentation rate to the bottom is with 4.0 to 4.9 g C m^{-2} d^{-1} higher next to the glacier than in the remaining Nordvestfjord. A negative *b* value (-0.57) and negative values for the remineralisation rate at 200 m depth indicate that the concentration of particles initially increases with depth.

3.4.2 Mid-Nordvestfjord pattern

At about 50 m depth, elevated nutrient concentrations compared to surrounding waters of the same depth (Fig. 3.6 and A.4) coincide with a patch of high nDIC and nTA values (Fig. 3.7a,b, 3.3a,c, and A.5a,b) at the surface. Surface pCO_2 values are the highest observed in the whole fjord with up to 720 µatm. The NCP is 26.5 to 31.7 mmol C m^{-2} d^{-1}. Between 50 and 100 m, the POC flux is increased to 0.6 to 0.8 g C m^{-2} d^{-1}, matching high turbidity values at approximately the same depth (Fig. 3.5a,b and A.3a,b). Low dissolved oxygen concentrations with almost 100 µmol kg^{-1} AOU can be found slightly deeper at 100 to 150 m depth (Fig. 3.4c, 3.7c, A.2c, and A.5c). One of the highest *b* values (0.55) is observed in this region, indicating a low sedimentation rate that coincides with a high remineralisation/lateral export rate within the top 200 m (122 to 145% of the NCP).

3.5 Sill region

Surface DIC and TA concentrations are pronouncedly lower at the surface just at the slope to Nordvestfjord. Contour lines of salinity indicate the upwelling of dense bottom water, whereas dissolved oxygen and heat are mixed downwards (Fig. 3.4). Nutrient concentrations are elevated close to the fresh surface layer, coinciding with a high POC flux of almost 1.0 g C m^{-2} d^{-1} (Fig. 3.6, 3.5b, A.4, and A.3b). NCP based on nutrient depletions is high with 64.4 to 78.8 mmol C m^{-2} d^{-1}. 86% of the NCP is remineralised within the upper 200 m, and only 0.1 g C m^{-2} d^{-1} POC reach the sea floor (*b* value: 0.28).
The sill seems to be an important obstacle controlling the exchange of bottom waters between the Outer Scoresby Sund and the Nordvestfjord, which can most obviously be seen in the temperature and AOU distribution, reflecting the different water masses (Fig. 3.4a and 3.7c).

3.6 Outer Scoresby Sund and shelf

Within the Outer Scoresby Sund, water masses coming into the fjord are clearly stratified. Cold Polar Water and and dense Greenland Sea Deep Water are separated by a layer of warm Atlantic Water. The deep water from the Greenland Sea carries a low concentration of dissolved oxygen of 260 µmol kg^{-1} (Fig. 3.4c), and together with the Atlantic Water it imports large amounts of nutrients into the fjord with concentrations up to 12 µmol l^{-1} nitrate+nitrite, 0.8 µmol l^{-1} phosphate, and 6.0 µmol l^{-1} silicate (Fig. 3.6).

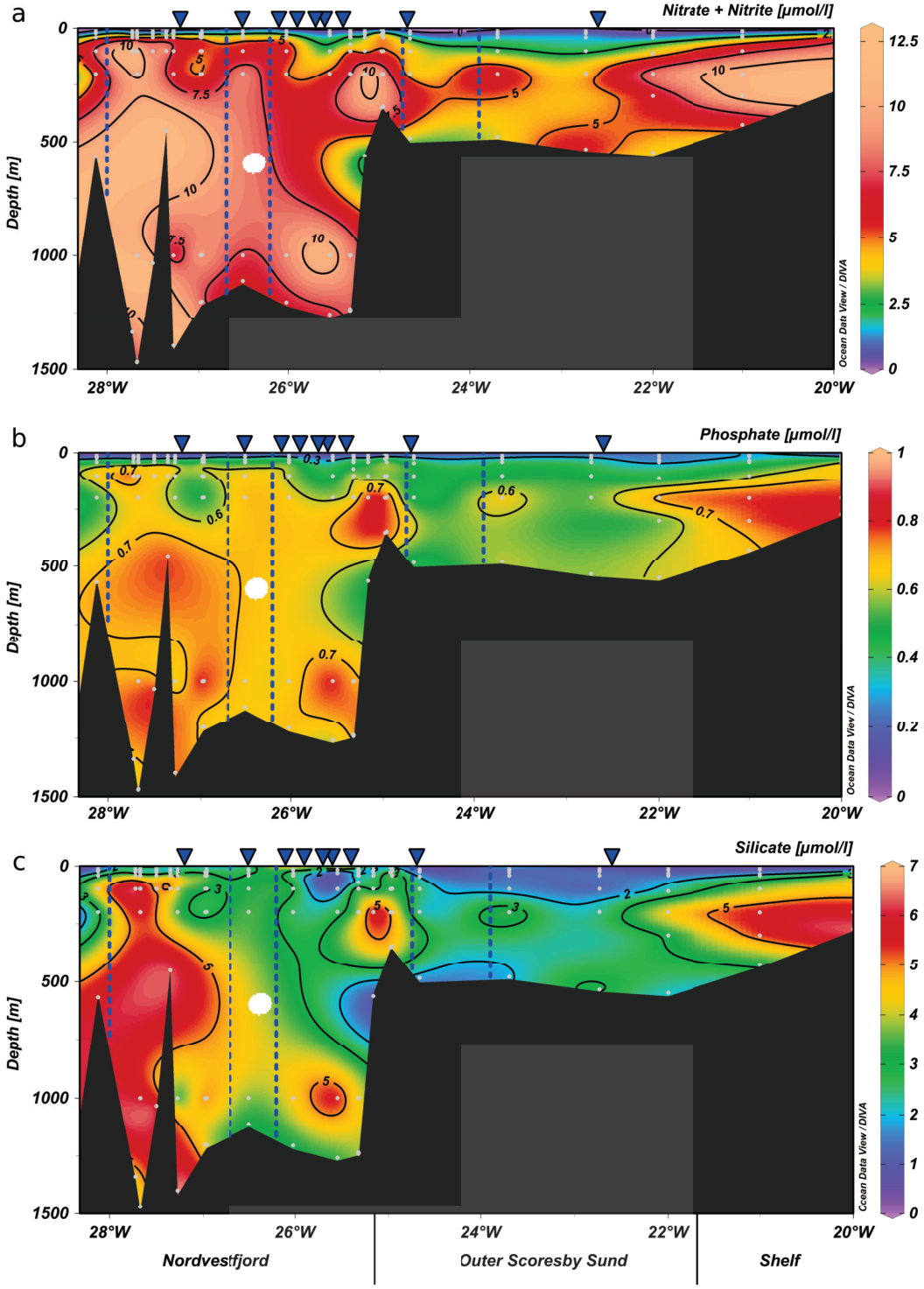

Figure 3.6: Nutrient concentrations ((a) nitrate+nitrite, (b) phosphate, (c) silicate) along the transect from the fjord head (left) to the fjord mouth (right). Labelling is similar to Fig. 3.4.

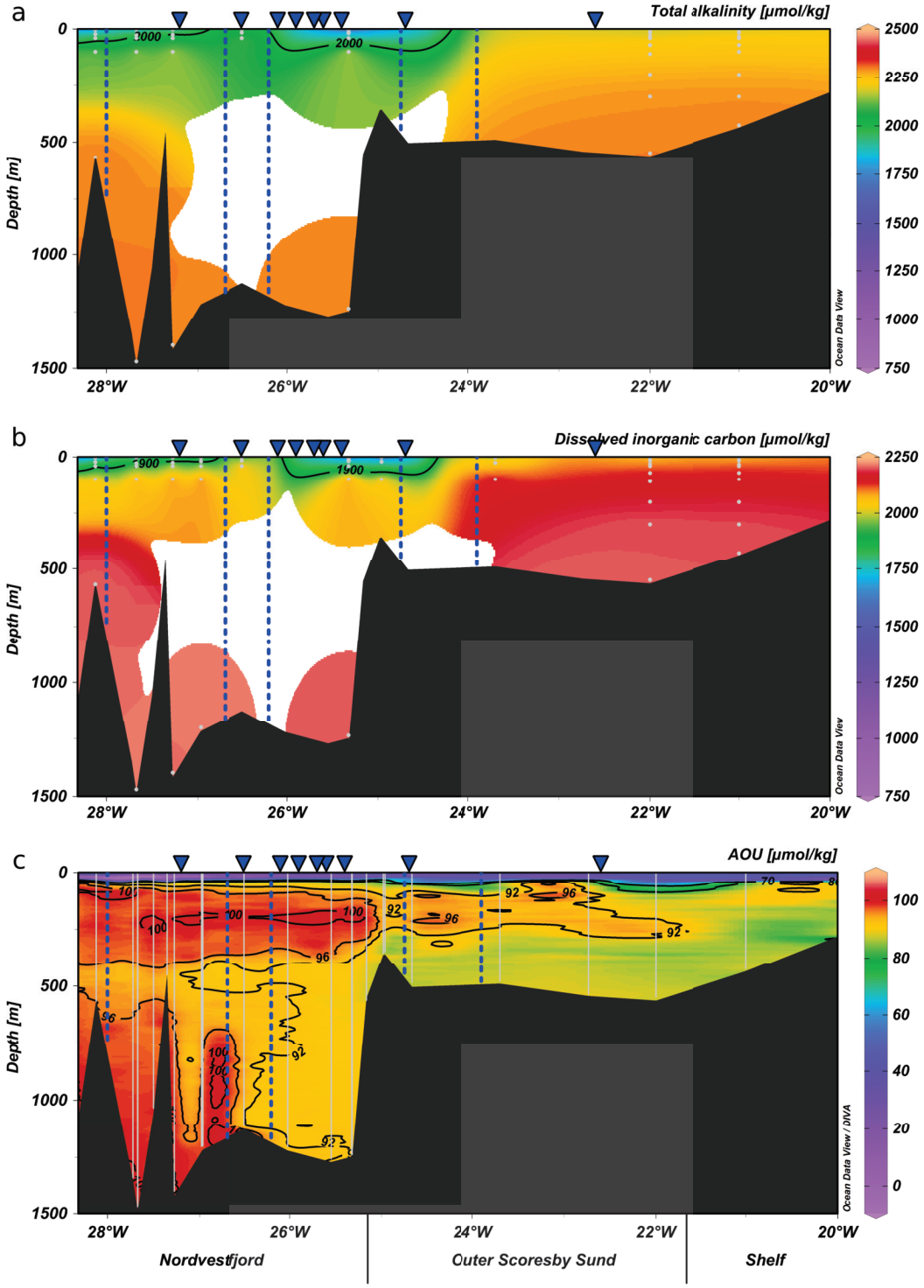

Figure 3.7: (a) TA, (b) DIC, and (c) apparent oxygen utilization (AOU) along the transect from the fjord head (left) to the fjord mouth (right). Labelling is similar to Fig. 3.4.

In the inner part of the Outer Scoresby Sund, the freshwater layer at the surface occupies the upper 10 m, but gets gradually thinner towards the fjord mouth and shelf. Temperatures are elevated to 2.5°C at the surface down to 15 to 20 m depth.

High turbidity patches within the upper 100 m (Fig. 3.5a and A.3a) match well with patches of high dissolved oxygen concentrations (Fig. 3.4c and A.2c), high fluorescence (Fig. 3.5c and A.3c), and low AOU (Fig. 3.7c and A.5c). Only one POC flux profile is available for this regional domain. POC flux varies between 0.1 and 0.2 g C m^{-2} d^{-1} (Fig. 3.5b).
Next to the obvious nutrient import by water from the shelf, a spot with elevated nutrient concentrations exists close to the marine-terminating glacier in Outer Scoresby Sund (Fig. 3.6). However, as this spot is only based on a single measurement, this feature will not be considered further.
TA and DIC increase gradually with depth and salinity (Fig. 3.7a,b).

NCP is higher in the Outer Scoresby Sund compared to Nordvestfjord with 42.2 and 67.3 mmol C m^{-2} d^{-1} for phosphate and nitrate+nitrite, respectively (Table 3.1). At the shelf, productivity is comparable with 52.0 and 61.9 mmol C m^{-2} d^{-1}. Negative values for the NCP based on DIC depletion (-36.1 and -124.2 mmol C m^{-2} d^{-1}, respectively) indicate an introduction of DIC into the system at the surface.
Remineralisation values are only available for the Outer Scoresby Sund. Remineralisation mainly takes place in the upper part of the water column, while only about 20% of the NCP reaches the sea floor.

Chapter 4

Discussion

4.1 General setting

The *Maria S. Merian* expedition in summer 2016 revealed that Scoresby Sund, a fjord influenced by marine- as well as land-terminating glaciers, can be separated into three regional domains with distinct differences in physical, biological, and biogeochemical parameters. The regime within the inner part of the fjord, Nordvestfjord, is governed by a highly variable bottom topography and the inflow of meltwater at the surface and at depth, whereas the shallower Outer Scoresby Sund is less mixed and mostly influenced by the dynamics of the tides. Both parts are separated by a wide sill, which has a distinct effect on the inflow of shelf water.

The circulation within the west Greenland fjord Godthåbsfjord, described by *Mortensen et al.* (2011), fits well to the patterns observed in Scoresby Sund, even though both fjords are influenced by different water masses and are slightly different in their bottom topography. Estuarine circulation and subglacial circulation (or buoyancy-driven circulation, a term used by other authors) establish because of surface and subglacial runoff, respectively. A relatively thin layer of freshwater at the surface and at depth transports waters out-fjord, building up an in-fjord directed compensation current in the water layers below. Currents established by the intermediate baroclinic circulation, by contrast, direct in-fjord at the surface and out-fjord at depth. It results from intense mixing due to tides and sills, leading to a downward flux of freshwater and heat. While in Godthåbsfjord, the shallower first part of the fjord is also characterised by steep sills and basins which lead to a strong intermediate baroclinic circulation, tidal influence and sills are regionally separated in Scoresby Sund. It is therefore assumed that in summer, the Outer Scoresby Sund is mainly governed by the intermediate baroclinic circulation as a reaction to tidal

currents, while buoyancy-driven circulation is prevalent in Nordvestfjord. The net transport direction of waters within the whole fjord depends of the density gradients due to mixing.

During winter, another circulation mode comes into play. Dense coastal inflow from the shelf is responsible for the exchange of water masses in the deep basins of the fjord, corresponding to the Nordvestfjord basin in Scoresby Sund. *Mortensen et al.* (2011) calculated a residence time of these waters of one to two years in Godthåbsfjord. However, residence times of deep waters in Greenland's glacial fjords in general are highly under debate and reach from months to decades (reviewed by *Straneo and Cenedese*, 2015). The age of the Atlantic Water filling the Nordvestfjord basin is therefore difficult to estimate. Either way, the AOU in the basin is high compared to the AOU in the freshly supplied Atlantic Water in the Outer Scoresby Sund, especially close to the bottom (Fig. 3.7c). Therefore, the ventilation rate of these waters cannot be high as it needs sufficient time to deplete the oxygen in this large water body. Recent changes in Atlantic Water characteristics (like warming) are therefore transferred with some delay into the deep Nordvestfjord basin, resulting in uncertain effects on the fjord's biological and biogeochemical system.

Buoyancy-driven circulation is the main conveyor of oceanic heat to the glacier in the inner part of the fjord, because it draws waters all the way to the fjord head (*Cowton et al.*, 2016). Other circulation modes, by contrast, are less effective in the exchange of waters in the inner part of the fjord. Basal melt of glaciers is additionally enhanced by geothermal heat forcing beneath the GrIS (*Rysgaard et al.*, 2018).

4.2 Surface pCO_2

The supersaturation of Scoresby Sund in terms of pCO_2 (Fig. 3.2) does partly contradict the observations in other Arctic regions and fjords (e.g., *Bates et al.*, 2006; *Cai et al.*, 2010; *Sejr et al.*, 2011; *Rysgaard et al.*, 2012; *Burgers et al.*, 2017), which were defined to be an important sink of atmospheric CO_2.

Undersaturation establishes because of a stable stratification that prevents upwelling of CO_2-rich bottom water (*Rysgaard et al.*, 2012), together with low surface water temperatures helping to maintain low pCO_2 (*Burgers et al.*, 2017). Especially in Nordvestfjord, however, no stable water mass stratification can be observed, because sills and submarine meltwater discharge lead to a mixing of the

water column, and also the water temperatures at the surface are different to those described by *Burgers et al.* (2017).
Upwelling, for example with melt plumes, can bring up high pCO_2 waters (*Mathis et al.*, 2012; *Rysgaard et al.*, 2012; *Meire et al.*, 2015). If these waters are supersaturated compared to the atmosphere, disequilibrium-driven outgassing can occur. Furthermore, warm surface waters with up to 12.5°C were prevalent in Nordvestfjord at the time of the cruise (Fig. A.2a), which can hold less CO_2 than cold waters. High water temperatures can significantly lower the gas solubility of the waters, which can partly compensate for the low pCO_2 due to glacial meltwater discharge, as observed in the northeast Greenland fjord Young Sound (*Rysgaard and Nielsen*, 2006).
The temperature and salinity distributions (Fig. 3.4a,b and A.2a,b) show that pCO_2 in Nordvestfjord has been measured within the surface meltwater layer which is heated by solar insulation. Strong stratification prevents mixing with deeper waters. High surface water temperatures might therefore be the main cause of pCO_2 supersaturation in Nordvestfjord. In the Outer Scoresby Sund, by contrast, the meltwater layer gets thinner and surface stratification less strong, making the intrusion of CO_2-rich waters to the surface possible.
pCO_2 in meltwater can additionally be highly dependent on the TA concentrations, with higher pCO_2 when TA concentrations are low (*Pilcher et al.*, 2018). The contribution of TA in the freshwater endmember is discussed in Section 4.3.1.
In addition to the physical factors, the influence of biology needs to be considered. *Burgers et al.* (2017) observed high (although still undersaturated) pCO_2 values in waters that are influenced by the input of silts, which limit production and, as a consequence, the drawdown of CO_2. In Nordvestfjord, production at the time of the cruise was low, and the fjord already in a post-bloom situation (further discussed in Section 4.3.1). This indicates that CO_2 drawdown is limited anyway and does not support an undersaturation in the surface layer.

pCO_2 values of 400 to 490 µatm (or even higher) are therefore in line with measurements in areas with enhanced upwelling (>500 µatm; *Rysgaard et al.*, 2012) and high surface temperatures (>670 µatm; *Reisdorph and Mathis*, 2015). At the shelf, in contrast, pCO_2 values with 400 ± 20 µatm are more or less at atmospheric level.

4.3 Nordvestfjord

Nordvestfjord is largely influenced by mixing due to a diverse bottom topography and strong meltwater input from marine- and land-terminating glaciers. This leads to the development of significant lateral advection, making it difficult to

attribute local features at the surface (like surface meltwater input or high primary productivity) to distribution patterns at depth.

Nonetheless, the sources of particulate matter measured as turbidity can clearly be identified (Fig. 3.5a and A.3a). At the surface next to large meltwater rivers as well as within the water column at the grounding lines of marine-terminating glaciers, high turbidity values show that particles are introduced with meltwater. Indeed, GrIS can carry a high load of particulate matter, which has the potential to limit primary productivity due to light attenuation (*Murray et al.*, 2015; *Arendt et al.*, 2016). The concentration of suspended sediment in meltwater differs significantly between catchment areas (*Hudson et al.*, 2014). As a second source, redistribution of particles from the sea floor increases the turbidity about 100 m above the bottom. Finally, phytoplankton at a depth of 25 m (measured as high fluorescence patches, Fig. 3.5c and A.3c) coincide with high turbidity.

4.3.1 Primary production

Primary productivity within high fluorescence patches can also be seen in the evolution of oxygen in the surface layer. Additionally, the surface discharge of meltwater supports the ventilation of the upper water column by bubble intrusion. While heat and freshwater are mixed downwards in the water column, dissolved oxygen decreases quickly within the upper 250 m (Fig. 3.4c). Low dissolved oxygen values can be attributed to an elevated remineralisation rate, indicated by a high AOU up to a depth of 400 m (Fig. 3.7c), and a long residence time of poorly ventilated Atlantic Water within the basin of Nordvestfjord.

Nutrient concentrations are relatively low in the upper 25 to 50 m due to primary production, whereas below this layer their concentrations are patchily elevated (Fig. 3.6). Previous studies showed that there is no consensus about the ability of meltwater from the GrIS to carry nutrients. While silicate is commonly believed to be transported into the system by glacial meltwater (*Meire et al.*, 2016a; *Hawkings et al.*, 2017), phosphate and nitrate contributions of meltwater to the fjord are currently under debate. *Wadham et al.* (2016) report the GrIS to be a nitrogen source to phytoplankton, whereas other investigators found elevated phosphate and nitrate concentrations in meltwater that are, however, not readily bioavailable (*Hawkings et al.*, 2015, 2016).
This study shows that at least the surface runoff of large meltwater rivers contains elevated concentrations of silicate, whereas nitrate+nitrite and phosphate concentrations are not elevated at this spot. At depth, concentration differences of silicate are comparable to those of the other nutrients, making it impossible to say

that also subglacial discharge imports silicate, but none of the other nutrients. From a geological point of view, it is possible that surface meltwater rivers take up silicate during their way across the bedrock, while submarine meltwater does not really get in contact with the bedrock surface, thus, does not accumulate significant amounts of silicate. However, lateral advection may mask the sources of nutrients so that elevated silicate (and other nutrient) concentrations cannot be attributed to certain positions of marine-terminating glaciers. A recent study demonstrated that GrIS meltwater does not increase nutrient concentrations directly, but that the meltwater plume from subglacial discharge induces the upwelling of nutrient-rich deep water to the surface, supporting a high primary production rate (*Meire et al.*, 2017). If this also holds true for Nordvestfjord, the distribution of nutrients is mainly determined by the upwelling of freshwater by marine-terminating glaciers throughout the fjord, bringing high nutrient concentrations from the basin water close to the surface. Low nitrate+nitrite and phosphate concentrations measured in waters of surface meltwater discharge all over Scoresby Sund support this assumption (Fig. 4.1).
Another important player in distributing nutrients are icebergs, which might contain a similar nutrient composition as glacial meltwater. They make up 30 to 50% of the freshwater loss from the GrIS, most of it being released at a depth of 100 to 300 m during summer (*Moon et al.*, 2017). Their contribution to the dispersal of nutrients and other substances is therefore presumably significant. Because they are widely distributed within the fjord and can hardly be localized, however, their impact can barely be quantified.

The relationship of nitrate+nitrite and phosphate in the temperature minimum (obtained by trapezoid integration of consecutive samples, Fig. 4.1) results in a high N:P ratio (approx. 23 N : 1 P) compared to the Redfield ratio (16 N : 1 P).
Remineralisation can shift the ratio of nutrients when one nutrient is remineralised faster than the other. *Tamelander et al.* (2012) described a more efficient retention of phosphorus compared to carbon and nitrogen within the upper water column due to a faster remineralisation of this nutrient. Ratios in the present study, however, show the opposite trend, meaning a faster remineralisation rate of nitrate+nitrite to phosphate. Another explanation could be that the N:P ratio of the phytoplankton assemblage in the fjord differs from the stoichiometric ratio of Redfield. Furthermore, different processes can change the nutrient concentrations within the mixed layer during winter (which is still present as winter remnant layer in summer). In comparison to phosphate, nitrate is more prone to be altered by other processes than phytoplankton growth, for instance denitrification and nitrogen fixation (*Anderson et al.*, 2003). Nitrate concentrations measured next to southern Greenland's glaciers can be highly variable and fluctuated by about

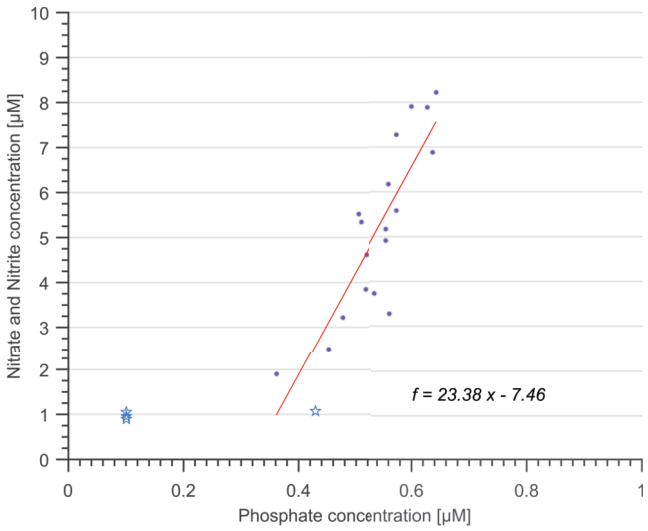

Figure 4.1: Relationship between nitrate+nitrite and phosphate concentrations across samples from the minimum temperature depth in Nordvestfjord. The function of the linear regression is given below the curve. Stars indicate concentrations of samples from surface meltwater runoffs in Nordvestfjord and Scoresby Sund.

4 µM within a two-weeks period (*Beaton et al.*, 2017). Also, the amount of nitrogen released from the ice depends on the time the ice was formed (*Wadham et al.*, 2016). All together, the above-mentioned processes can lead to deviations of the nutrient composition from the Redfield ratio within the winter remnant layer. Further investigations are needed to clarify these deviations in more detail. In principle though, production limited by nitrate prior to phosphate is a common phenomenon in Greenland fjords as well as in Arctic waters in general (*Harrison and Cota*, 1991; *Rysgaard et al.*, 2003; *Juul-Pedersen et al.*, 2015).
Overall, it seems that meltwater does not change nitrate+nitrite and phosphate concentrations considerably in the first place, but might have an influence on their distribution by rising meltwater plumes, which is in line with observations in other Greenland fjords (*Meire et al.*, 2016a, 2017).

NCP estimates can fluctuate due to different assumptions made during the computation process. Different initial concentrations based on the variability of shelf concentrations in the winter remnant layer can result in NCP estimates deviating by ±18% (from nitrate+nitrite depletions) and ±41% (from phosphate depletions), from the ones presented here. If not a trapezoid integration is applied, but constant values per depth interval are assumed, NCP estimates can even vary by ±70%. The overall variability is, however, believed to be lower, as a gradual increase or decrease of nutrient concentrations from one sampling depth to the other is more probable than stepwise changes.

The NCP calculated from nutrient deficits (30.9 to 34.7 mmol C m^{-2} d^{-1}) is in good agreement with literature values. In Glacier Bay, Alaska, *Reisdorph and Mathis* (2015) determined a production rate of 54 to 81 mmol C m^{-2} d^{-1}, which is higher than the production rates of the present study. Production might be limited by a thin, but stable freshwater layer at the surface, preventing the replenishment of the upper meters with nutrients (Fig. A.2b). Sealing of nutrients at depth due to the stability of the water column was also observed in Young Sound further north (*Rysgaard and Nielsen*, 2006), resulting in lower phytoplankton biomass compared to areas with less surface meltwater discharge (*Middelbo et al.*, 2018). Due to their large surface-area-to-volume ratio, smaller phytoplankton is favoured in low-nutrient surface freshwater (*Li et al.*, 2009; *Middelbo et al.*, 2018). Additionally, silts within the meltwater might have a shadowing effect, thus, decreasing light penetration and therefore primary productivity.
While open water areas of polar regions, like the basin of Chukchi Sea, the Arctic Ocean basin, and the Weddell Sea and Drake Passage in Antarctica, generally experience ten to one hundred times lower export production rates (*Hoppema et al.*, 2000; *Anderson et al.*, 2003; *Bates et al.*, 2005; *Hoppema et al.*, 2007; *Mathis et al.*, 2009; *Munro et al.*, 2015), shelf areas of the Chuckchi Sea and the Larsen Shelf are with about 80 to 250 mmol C m^{-2} d^{-1} more productive than the Nordvestfjord (*Hoppema et al.*, 2000; *Bates et al.*, 2005; *Mathis et al.*, 2009). It can be assumed that production has come to an end at the time of the cruise, because visual analyses of net samples revealed that the phytoplankton community was already in the post-bloom stage (B. Edvardsen, pers. comm.). Much debris, many copepods and fecal pellets found in the sediment traps (H. van der Jagt, pers. comm.) show that intense grazing already diminished the primary production. This is supported by the low fluorescence at the surface of 2.5 to 5 µmol l^{-1} compared to 10 to 15 µmol l^{-1} in Godthåbsfjord in August (*Meire et al.*, 2015).
A NCP of -0.3 mmol C m^{-2} d^{-1} based on the deficits of DIC reveals that waters in the winter remnant layer contain less dissolved CO_2 than the upper water layers. Factors leading to a high pCO_2 (Section 4.2) might also lead to higher DIC concentrations at the surface. This indicates that DIC is not an appropriate parameter for the determination of NCP.

The DIC and TA concentrations at zero salinity (determined by linear interpolation of the relationships between DIC/TA and salinity, Fig. A.1) with 423.13 and 726.45 µmol kg^{-1}, respectively, are remarkable. There are some uncertainties in this approach, because surface samples with salinities below 30 have been excluded from the linear interpolation as they might have been changed by biological processes. Other studies found profoundly lower freshwater endmember concentrations of

about 160 μmol kg^{-1} for TA and 60 to 160 μmol kg^{-1} for DIC in the west Greenland fjord Godthåbsfjord with similar methods (*Rysgaard et al.*, 2012; *Meire et al.*, 2015). Generally, however, it is known that the GrIS contains dissolved CO_2 which is transferred into the ocean and the atmosphere by melting of glaciers (*Ryu and Jacobson*, 2012). With respect to TA, the source of meltwater is important. Discharge from land-terminating glaciers carries higher TA concentrations due to stronger interaction with the bedrock than the meltwater from marine-terminating glaciers (*Brown*, 2002; *Pilcher et al.*, 2018). Thus, the share of meltwater originating from land is possibly higher in Scoresby Sund than in Godthåbsfjord.

Normalising DIC and TA to a constant salinity (nDIC and nTA, respectively) visualises the effects of production, remineralisation, and calcium carbonate dynamics by excluding the dilution effect. While samples with a relatively high salinity have almost constant nDIC and nTA concentrations, the concentrations in low-salinity samples, originating from surface waters in Nordvestfjord, are more variable (Fig. 3.3).

In most cases, nTA at the surface is lower than the mean nTA of the deeper samples, indicating the precipitation of carbonate minerals. However, only few calcifying species, like coccolithophores, were found via visual inspection in net samples (B. Edvardsen, pers. comm.). It is therefore assumed that a different mechanism apart from the one based on biological processes changes the carbonate dynamics.

A sufficiently high concentration of ions in the brine channels of ice can lead to the anorganic production of calcium carbonate, mainly in the crystalline form of ikaite. This process decreases DIC and TA in the brine, but increases pCO_2 (*Rysgaard et al.*, 2009; *Jones et al.*, 2010). When the ice melts, the brine is released to the surface layer, lowering the nTA concentration of the surface water (and increasing pCO_2, an effect that can indeed contribute to the surface pCO_2 variability described in Section 4.2). Strikingly, the concomitant trend in nDIC is more diverse and indicates not only a depletion, but also an increasing concentration of DIC at the surface. Thus, other factors like air-sea gas exchange and primary production must have had an effect on the surface DIC budget. This is supported by the fact that ice breakup already had occurred about one month before and that the time frame was sufficiently long for such processes. Also, rising meltwater plumes from submarine glacial discharge can bring up low-DIC waters (*Meire et al.*, 2015). The observation of *Rysgaard et al.* (2012), that elevated TA values relative to DIC show the contribution of carbonate minerals with glacial melt, can therefore not be confirmed, as it would require that no other processes have an effect on the TA and DIC concentrations.

Low nTA values at the surface can have a direct impact on the carbon cycling in the Nordvestfjord. First, a similar production at low salinities and low TA has a stronger effect on pCO_2 than in more saline and TA enriched waters, increasing

the ability of the fjord waters to be a CO_2 sink (*Meire et al.*, 2015). Second, low TA concentrations can reduce the buffering capacity of the waters in terms of pH and, thus, the aragonite saturation state (*Reisdorph and Mathis*, 2014). Aragonite is a crystalline form of calcium carbonate, and is mainly formed by pteropods. As a consequence, low saturation states can significantly influence the biodiversity in the fjord.

4.3.2 Carbon flux and remineralisation

Close to glacier fronts, POC fluxes are high with 0.5 to 2 g C m^{-2} d^{-1}, while in the remaining Nordvestfjord, POC fluxes are maximal 0.1 to 0.3 g C m^{-2} d^{-1} (Fig.3.5b). The distinct flux pattern of Daugaard-Jensen glacier is discussed in more detail in Section 4.3.3. Generally, the POC fluxes in direct vicinity to glacier fronts correspond to observations in Adventfjorden, Svalbard, with 0.77 to 1.53 g C m^{-2} d^{-1} (*Wiedmann et al.*, 2016). But also the fluxes in the remaining Nordvestfjord coincide with depth-integrated values of 0.2 to 1.1 g C m^{-2} d^{-1} in Adventfjorden (*Wiedmann et al.*, 2016), Svalbard, and annually-integrated fluxes of 0.65 g C m^{-2} d^{-1} in Kobbefjord, southwest Greenland (*Sørensen et al.*, 2015).

A clear pattern as observed in many open ocean POC profiles with a large decrease at the surface due to zooplankton grazing and a smaller, but steady decrease at depth by microbial remineralisation (*Iversen et al.*, 2010; *Belcher et al.*, 2016), cannot be found here. By contrast, POC fluxes are increasing and decreasing with depth without any clear trend. Input of lithogenic material with meltwater of marine-terminating glaciers as well as lateral advection of these plumes might be responsible for the highly variable fluxes with depth. Furthermore, particles can accumulate at density gradients (*Alldredge and Crocker*, 1995), which can also contribute to the unequal distribution of POC in the water column, just as the active transport of carbon by vertically-migrating zooplankton (reviewed by *Turner*, 2015). If these organisms actively enter the sediment traps, they might additionally bias the estimate of organic carbon fluxes. The variability between stations in Nordvestfjord is very high, resulting in a standard deviation of ± 0.43 for the b value. Calculations of the remineralisation with depth should therefore be taken with caution.

On average, only 12 to 20% of the NCP calculated from nutrient depletion is remineralised (or exported horizontally) within the upper 200 m, whereas more POC is sedimenting onto the sea floor per day than produced from the NCP. However, the daily NCP rate was calculated based on the number of open water days since winter and averages out fluctuations in production within this period. Thus, the daily production must not necessarily fit to the daily flux. Additionally,

sinking speeds of only about 10 m per day for the most prevailing particle size of 200 µm (H. van der Jagt, pers. comm.) shift the events at the surface and the fluxes at depth several days apart. Generally, however, the *b* value, which constitutes the carbon export efficiency, is comparably low compared to the global value of 0.86 (*Martin et al.*, 1987) and to the values proposed by *Guidi et al.* (2015) for Arctic provinces (1.65 - 1.75). This means that Nordvestfjord can indeed be a spot of high carbon sedimentation, or even carbon burial like proposed by *Smith et al.* (2015) for fjords in general.

Why is sedimentation so high close to glacier fronts, but by five times lower in the remaining Nordvestfjord?
The meltwater from the GrIS has a high sediment and solute concentration, mainly because of its passage along the ice bed interface (reviewed by *Nienow et al.*, 2017). It has been proposed several times that silts present in meltwater from glaciers might ballast particles and, thus, increase the sinking velocities (e.g., *Iversen and Robert*, 2015; *Wiedmann et al.*, 2016). Sinking velocities are the main driver determining the efficiency of the biological carbon pump (*Ploug et al.*, 2008; *Iversen et al.*, 2010), and settling rates are dependent on the prevailing local environment in which particles are formed (*Nowald et al.*, 2009). It therefore seems plausible that meltwater from the Daugaard-Jensen glacier as well as other marine-terminating glaciers plays a crucial role in the high export efficiency within Nordvestfjord. The observation of a high silt load in gel traps of the Snow Catcher which was deployed next to Daugaard-Jensen glacier (H. van der Jagt, pers. comm.), supports this. Incidentally, particles were not smaller because of fragmentation into pieces when ballasted with silts, as proposed by *Passow and De La Rocha* (2006) and *Iversen and Robert* (2015).
Another point that needs to be considered is the timing of the camera profiles for particle recordings. Due to dial cycles in production and grazing by plankton, vertical particle flux might change during the coarse of the day. *Petrik et al.* (2013) observed evening highs and morning lows in the integrated particle load. Due to intense vertical and lateral mixing of the water column, no such picture could be seen in the profiles of the present study. However, another profile schedule with regard to the day time could have resulted in different fluxes, hence, this variation needs to be kept in mind.

4.3.3 Daugaard-Jensen glacier

Daugaard-Jensen glacier is one of the largest east Greenland glaciers with a drainage basin of about 50 150 km^2 (*Rignot and Kanagaratnam*, 2006). Its surface meltrate is relatively low compared to other Greenland glaciers (mean 0.0014 m d^{-1}), whereas the rate of submarine melt is considerable with a mean of 2.41 m d^{-1} (*Enderlin and Howat*,

2013). The position of the Daugaard-Jensen glacier's front is highly variable within the year compared to other Greenland glaciers, while the inter-annual mean front position has not changed from 2000 to 2010 (*Walsh et al.*, 2012; *Enderlin and Howat*, 2013).

The closest station has a distance of about 12 km to the glacier's front. At the surface where large meltwater discharge takes place, the lowest pCO_2 values of the whole fjord were observed within an area of about 25 km away from the terminus (Fig. 3.2). *Meire et al.* (2015) found two reasons for that. First, meltwater itself can be undersaturated in terms of pCO_2. Second, the mixing of fresh and saline water leads to a non-conservative behaviour of pCO_2 in the resulting water mass. The most pronounced undersaturation can generally be found at a salinity of 8. The waters at the closest stations to Daugaard-Jensen at the depth of the surface pCO_2 measurement (about 6.5 m depth) have a salinity of 20. Nevertheless, pCO_2 can be lowered by this mechanism. Ultimately, this undersaturation means that large glacial meltwater discharge like observed at the Daugaard-Jensen glacier can promote the uptake of CO_2 into the ocean.

A salinity drop by 0.1 to 0.2 units at 200 to 250 m depth at the closest station to the glacier front of the Daugaard-Jensen glacier indicates the position of the plume formed from submarine meltwater discharge. Submarine melt mostly occurs at the base of tidewater outlet glaciers from large discharge channels, but can also be amplified by numerous smaller discharge outlets distributed across the glacier terminus (*Bendtsen et al.*, 2015; *Fried et al.*, 2015). Basically, the pattern of subglacial discharge, which has an effect on the distribution and size of meltwater plumes, is largely unknown for all marine-terminating glaciers (*Straneo and Cenedese*, 2015; *Stevens et al.*, 2016), and for the Daugaard-Jensen glacier in particular. Besides, Daugaard-Jensen glacier has a significant interannual variability in submarine melt (*Enderlin and Howat*, 2013). The pattern and amount of Daugaard-Jensen's submarine discharge can therefore barely be amplified.

A high turbidity plume can be observed about 50 m above the low-salinity plume, whereas POC flux is increased about 50 m below it (Fig. A.3a,b). Because the meltwater plume is believed to rise towards the surface while mixing with the fjord water, small particles that can be detected as turbidity follow this distribution. Meltwater plumes do not necessarily reach the surface, but can also attain neutral buoyancy at another depth (*Stevens et al.*, 2016). Even though different tidewater glaciers in fjords may have completely different conditions regarding the entrainment of meltwater plumes, it is believed that the initial plume velocities estimated for an Alaskan fjord can be more or less transferred on Daugaard-Jensen glacier, accounting for 6 to 15 m s^{-1} (*Mugford*

and Dowdeswell, 2011). Because melting at the glacial front is thought to having started earlier within the year, a meltwater plume that has a comparable initial velocity would have already reached the surface. Thus, it can be assumed that this meltwater plume does not reach the surface, but is rather trapped at a depth of 100 m due to the density of the surrounding waters. The small particles do accumulate at this depth before they gradually fall out, displayed by a trace of elevated concentrations down to 350 m depth. Low nutrient concentrations at the same depth suggest that the meltwater does hardly introduce any nutrient (Fig. A.4).

Because only particles with a minimum size of 20 µm were recorded during the POC flux analysis, its profiles do not cover the silt export described before. Thus, the depths of the POC flux maximum and the turbidity maximum in the vicinity of the glacier front do not coincide. High POC flux cannot be the result of a high export production at the surface, as the NCP is not significantly higher at the stations close to the Daugaard-Jensen glacier than in the remaining Nordvestfjord. Also, the particle concentration is higher below the photic zone and results in a high sedimentation rate down to the bottom. This indicates that factors other than primary production are responsible for the high concentration of particles within the upper 250 to 400 m. Meltwater from glaciers can induce mass mortality of zooplankton (*Węsławski and Legeżyńska*, 1998). Carcasses that are sinking out, and that are potentially aggregated and ballasted by meltwater sediments, could have the potential to increase the POC flux considerably. Besides, glacial melt itself could entrain particulate organic matter, as assumed by *Wiedmann et al.* (2016) in Adventfjorden, Svalbard. At about 350 m depth, particles are laterally advected away from the meltwater plume. This advection coincides with the depth of the Atlantic Water/Polar Water interface and potentially highlights the out-fjord directed current of the buoyancy-driven circulation described in section 4.1.

It has to be considered, though, that subglacial discharge in general is most prominent in direct vicinity to the glacier front (~5 km), whereas the influence of the plume-entrainment decreases considerably within 20 km distance to the glacier (*Bendtsen et al.*, 2015). The plumes described above span a distance of at least 20 to 25 km from the glacier's front. This could be the reason why the plume entrainment can barely be seen in temperature distributions, while the concentrations of other tracers like nutrients and particles do still differ from the surrounding waters even further away from the terminus. To get a better insight into the spatial distribution of temperature, salinity, and other tracers closer to Daugaard-Jensen's glacier terminus, observations with autonomous underwater vehicles, like performed by *Stevens et al.* (2016), could be a valuable tool.

4.3.4 Mid-Nordvestfjord pattern

A very specific distribution pattern of dissolved matter and POC fluxes can be seen between 26 and 27°W.

Fluorescence is not particularly elevated at the surface (Fig. A.3c), and the NCP is in the range of the remaining fjord. In the upper 50 m of the water column, elevated nutrient and nDIC concentrations as well as pCO_2 values (Fig. A.4, 3.3a, and 3.2) point towards active remineralisation processes. Correspondingly, AOU is low at depths that are not mixed with the well-ventilated surface waters (Fig. A.5c), and the *b* value is with 0.55 comparatively high, indicating an effective decrease of carbon within the upper ocean.
High nTA concentrations of about 2800 µmol kg^{-1} at the low-salinity surface are contradictory to the trend within the remaining Nordvestfjord, where surface nTA concentrations are lower than at depth (Fig. 3.3c). Hence, carbonate mineral dissolution seems to take place. High nDIC concentrations and high pCO_2 (Fig. 3.3a and 3.2) might lower the saturation state of carbonate minerals and increase their probability to dissolve.

There is no indication that the general setting of this area differs significantly from the remaining fjord, neither in terms of meltwater discharge, nor with regard to the length of the period of open water or a connection to other fjords. However, everything points towards a recently terminated bloom and the subsequent export of high amounts of organic carbon. Strikingly, even if marine-terminating glaciers are influencing this location, a ballasting by minerals and a resulting quick flux to depth cannot be observed.
If such a pattern could also be seen in other locations of the fjord at a different time, or if it is unique for this special location because of any physical and/or biological presetting, remains unknown.

4.4 Sill region

Low TA and DIC concentrations at the surface just above the sill (Fig. 3.7a,b and A.5a,b) can be attributed to the intense meltwater inflow from several discharge rivers further up-fjord. This surface water is then transported towards the fjord mouth by buoyancy-driven circulation, drifting the low-TA and low-DIC plume further away from the position of the discharge rivers.

The separation of Outer Scoresby Sund and Nordvestfjord by a sill is some-

what comparable to the bottom topography of Stjernsund, a sound in northern Norway. The sound is divided by a sill with a crest at about 200 to 240 m water depth. Internal wave formation by unidirectional currents coming into the sound leads to vertical mixing processes at the coastward side of the sill (*Rüggeberg et al.*, 2011).
Current regimes in Nordvestfjord have to be investigated further, but if they are comparable to those described by *Mortensen et al.* (2011) in Godthåbsfjord, the in-fjord directed compensation current resulting from the buoyancy-driven circulation could create similar internal waves. Thus, waters below the surface layer are highly turbulent, while the surface itself is less affected by the mixing processes. Nutrients can therefore reach the photic zone and promote primary production (Fig. 3.6 and A.4). While fluorescence was not significantly elevated at the time of the cruise (Fig. A.3c), NCP is one of the highest in the whole fjord. POC flux is high with almost 1 g C m^{-2} d^{-1}, but decreases quickly within the upper water column (Fig. 3.5b), indicating active remineralisation. Consistently, pCO_2 is with 550 to 650 µatm higher than compared to most areas within the remaining fjord (Fig. 3.2). Similar to the mid-Nordvestfjord pattern (Section 4.3.4), it is believed that this region recently experienced a phytoplankton bloom, that terminated shortly before it was sampled.

The sill is especially important for the deep water exchange between Outer Scoresby Sund and Nordvestfjord. While the part of the Outer Scoresby Sund that is closer to the fjord mouth is slightly deeper than the sill, Greenland Sea Deep Water at the bottom does not reach the Nordvestfjord and is trapped by the sill. Consequently, the Nordvestfjord basin is mainly filled by the shallower Atlantic Water. Because of its enormous size, it is probable that it takes several seasons until the basin water is exchanged. For estimating the effect of "old" water on different parts of the carbon cycle, but also for analysing the effect of a warming Atlantic Water source, it would be important to do further investigation on this water mass.

4.5 Outer Scoresby Sund and shelf

Because of its considerable width, meltwater discharge to the Outer Scoresby Sund has a considerably lower impact on the regimes in this region. Waters resemble those of the Greenland shelf. Salinity and temperature profiles reveal that interfacial mixing between the water masses occurs. However, no extensive mixing can be observed, probably due to the absence of steep sills and deep basins. This is supported by the TA and DIC concentrations which gradually increase with salinity and depth. Hydrography is therefore likely dominated by tides and intermediate baroclinic circulation.

4.5.1 Primary production

Three well-defined high fluorescence patches at the fjord mouth and the shelf (Fig. A.3c) coincide clearly with patches of high turbidity (Fig. A.3a), high dissolved oxygen concentrations (Fig. A.2c), and low AOU concentrations (Fig. A.5c), which demonstrates three things. First, turbidity measurements record solely high plankton concentrations, and silts or sediments from glacial meltwater seem not to be abundant in this region. Second, the upper two patches have the highest fluorescence values observed in Scoresby Sund; this matches with the observation of healthy and thriving phytoplankton communities in net samples (B. Edvardsen, pers. comm.). Third, a third patch can be identified at about 100 m depth. Shadowing by silts which decreases the light penetrations is barely existing, though.
High fluorescence patches are not mirrored in low nDIC concentrations at the same depths (Fig. 3.3b). The reason could be that sampling frequency for DIC was not dense enough to cover these spots.

Within the Outer Scoresby Sund, NCP computed from nutrient depletions increases towards the fjord mouth, with a mean production between 43.2 and 67.3 mmol C m^{-2} d^{-1}. Nutrients are imported by Atlantic Water and Greenland Sea Deep Water from the shelf, increasingly fuelling the surface layer the thinner the meltwater layer gets towards the fjord mouth. Due to interpolation reasons, the assignment of high nutrient concentration to a water mass is difficult on the section plot in Fig. 3.6, but the T/S plot in Fig. A.6 reveals more accurate information.
Production has not finished yet at the time of the cruise, which is why NCP can be underestimated. Interestingly, this does not coincide with observations in Godthåbsfjord, where the bloom in the inner fjord occurs later than further out-fjord because the ice cover lasts longer (*Hopwood et al.*, 2016). In Scoresby Sund, however, ice break-up happens up to 15 days earlier in Nordvestfjord compared to the Outer Scoresby Sund.

At the shelf, NCP is comparable to the production in the Outer Scoresby Sund. Because pCO_2 at the shelf is less variable than observed in Nordvestfjord and the sill region, the air-sea gas exchange is probably mainly governed by winds (*Andersson et al.*, 2017) and by drawdown due to primary production.

4.5.2 Carbon flux and remineralisation

With -36.1 and -124.3 mmol C m^{-2} d^{-1}, the NCP estimate based on the deficits of DIC is substantially different to the above-mentioned ones. POC flux is high at

the depth of high fluorescence and down to 75 m (Fig. 3.5b and A.3b). It seems as if the border between the fresh meltwater at the surface and the slightly more saline Polar Water acts as a trap of particles, that accumulate at this density gradient. This phenomenon has previously been described by *Alldredge and Crocker* (1995). Below this gradient, the concentration of particles is mainly determined by the water mass, where Polar Water carries low concentrations, and Atlantic Water and Greenland Sea Deep Water carry slightly elevated POC concentrations. The same might be true for DIC concentrations, with different water masses holding different concentrations of DIC, and replenishment of the surface with CO_2 by one water mass masking the effect of CO_2 drawdown by primary production.

Remineralisation is highly effective at the surface. NCP decreases by 73 to 91% within the upper 200 m in the Outer Scoresby Sund, and the mean b value is with 0.34 ± 0.11 three times higher than in Nordvestfjord. Fragmentation and ingestion by zooplankton in the upper water column is an important mechanism to increase flux attenuation significantly, together with the timing of the bloom (*Belcher et al.*, 2016). The fresh surface in Outer Scoresby Sund is considerably thinner than in Nordvestfjord, and is, thus, more favourable for zooplankton that is feeding on the thriving phytoplankton bloom. The density gradients described above give the zooplankton additional time to feed effectively before particles are sinking to a depth were microbial respiration dominates over zooplankton activity.

Chapter 5

Conclusion

5.1 Summary

Based on the research questions and hypotheses that were mentioned in the introduction, the following concluding statements can be made:

1. Surface heating by solar insulation and local upwelling of CO_2 rich water establish CO_2 outgassing in large parts of the fjord. Large amounts of meltwater, by contrast, for example in direct vicinity of marine-terminating glaciers, lead to undersaturation and the associated CO_2 uptake by the surface waters. Signals in the distribution patterns of dissolved and particulate matter caused by the largest marine-terminating glacier in Scoresby Sund, the Daugaard-Jensen glacier, can be seen up to 25 km away from the glacier front.
Even if the freshwater endmember concentrations are relatively high compared to other regions, DIC and TA concentrations in meltwater are clearly lower than in the deep fjord water. Accordingly, DIC and TA are diluted by the inflow of meltwater. Nevertheless, both parameters are not only conservatively influenced by salinity changes, but do also experience non-conservative behaviour at the surface in Nordvestfjord, mirroring the effects of production, remineralisation, and carbonate mineral dynamics. In the Outer Scoresby Sund, however, the high NCP and the persistent bloom during the cruise are not displayed in lower DIC concentrations at the surface compared to deeper waters.

2. In Nordvestfjord, marine-terminating glaciers, surface meltwater discharge, and the characteristic bottom topography promote upwelling and lateral advection of deep water masses. The fresh surface layer in the upper 10 m prevents, however, nutrients to reach the surface, and silts within the meltwater decrease the light

penetration. Meltwater does not import nutrients, except for surface meltwater discharge which contains elevated concentrations of silicate. Consequently, NCP is low compared to the Outer Scoresby Sund and the shelf, where the import of nutrients with Atlantic and Greenland Sea Deep Waters fuels the system. Besides, ice breakup starts some days earlier in Nordvestfjord than in the Outer Scoresby Sund, coinciding with an ongoing bloom in the Outer Scoresby Sund and a post-bloom situation in Nordvestfjord. NCP of the Outer Scoresby Sund could therefore be underestimated. The role of icebergs in the whole system in general is unknown, as they can barely be quantified and localized.

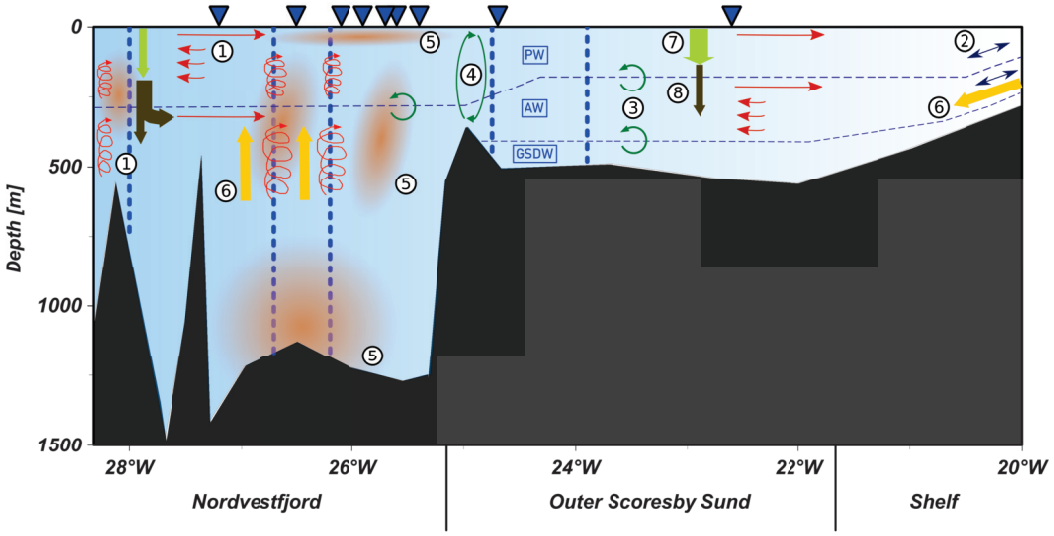

Figure 5.1: Conceptual figure of the different regimes in Scoresby Sund influencing the fjord carbon cycle. Current regimes proposed for Scoresby Sund are (1) buoyancy-driven circulation composed out of surface and submarine discharge, rising meltwater plumes, out-fjord directed currents and in-fjord directed compensation currents; (2) intermediate baroclinic circulation, and (3) interfacial mixing between water masses. Currents, bottom topography, and meltwater discharge result in (4) a well mixed water column at the sill, (5) plumes of high turbidity at the depth of surface and submarine meltwater discharge as well as by resuspension, and (6) upwelling of nutrients in Nordvestfjord and import by Atlantic and Greenland Sea Deep Water Water from the shelf. Arrows of (7) export production and (8) POC flux are scaled to the according magnitude, while the bent arrow of the export production in Nordvestfjord shows the lateral advection of particles following the buoyancy-driven circulation. PW = Polar Water, AW = Atlantic Water, GSDW = Greenland Sea Deep Water.

3. Glacial melt contains silts that enhance the vertical export by ballasting. Accordingly, particles in Nordvestfjord are barely remineralised in the upper water column, but rather exported to depth where they are either buried or remineralised in the sediment. The strong lateral advection (for example by the buoyancy-driven

circulation) and the proposed input of particles with glacial meltwater does, however, mask the source and fate of particles, as it partly leads to increasing POC fluxes at depth. Besides, POC flux close to glacier termini is probably independent from the production at the surface, as the flux can also be enhanced by mass mortality of plankton in the meltwater plumes.
In the Outer Scoresby Sund, POC flux is mainly dependent on the water mass feeding the fjord. On the one hand, Atlantic Water contains a priori a higher concentration of particles. On the other hand, particles can settle at density gradients and are therefore more prone to be remineralised in the upper water column. This is why the POC flux decreases considerably in the upper 200 m of the Outer Scoresby Sund and just a small fraction of it reaches the sea floor. Different to Nordvestfjord, the Outer Scoresby Sund can therefore not be seen as a hotspot of carbon burial.

Overall, carbon cycling in Nordvestfjord and the Outer Scoresby Sund is governed by considerably different regimes in terms of currents, input of particulate and dissolved material, and meltwater discharge. The sill between both regional domains plays an important role in separating the water masses and in creating an own dynamic environment with regard to production and carbon export. Fig. 5.1 summarizes the main outcome of this study.

5.2 Outlook

Ongoing climate change triggers shrinking sea ice cover, increasing glacial melt, and higher water temperatures, and will therefore cause major changes in the polar regions. Coastal ecosystems like Arctic fjords are especially prone. However, they are highly understudied (reviewed by *McKinley et al.*, 2017) and one can only speculate how these ecosystems will react on the different effects accompanying climate change.

Surface melt of the GrIS has increased dramatically since the year 2000, resulting from warmer air temperatures and a reduced albedo of the darkening ice sheet surface at the ablation zone (*Nienow et al.*, 2017). The retreat of marine-terminating glaciers, on the other hand, is not necessarily caused by the warming atmosphere, but rather by the transport of heat towards the glacier's termini (*Walsh et al.*, 2012; *Enderlin and Howat*, 2013; *Carr et al.*, 2017) as well as other factors, like the nature of the meltwater plume (reviewed by *Straneo and Heimbach*, 2013). Buoyancy-driven circulation as the main conveyor of heat transports warm Atlantic Water to the glaciers, resulting in an accelerated glacier retreat and an increased submarine meltwater discharge. This growing amount of meltwater in

turn increases the magnitude of the buoyancy-driven circulation and the therefore the glacial melting rate, resulting in a positive feedback cycle (*Sørensen et al.*, 2015; *Cowton et al.*, 2016).
Waters of the subpolar North Atlantic have been warming rapidly since the mid-1990s, along with a substantial thickening of the Atlantic layer. Thus, fjord waters are significantly influenced by those warm waters, which can reach the fjord heads due to scarce along-fjord variations in the water masses (reviewed by *Straneo and Heimbach*, 2013; *Straneo*, 2017). Recently, increasing water temperatures of the Atlantic layer have been measured close to the 79NG in north-east Greenland (*Schaffer et al.*, 2017). Overall, it has to be expected that the discharge of meltwater to Greenland's fjords will significantly increase. These freshwaters were identified to be retained within the southward flowing coastal currents and do therefore contribute to the freshwater content in the Subarctic Atlantic Ocean, influencing the deep water formation in this area (*Sejr et al.*, 2017).

What does all that ultimately mean for the world's largest fjord system, Scoresby Sund, and its future carbon cycle?

I. If the share of meltwater from land-terminating glaciers is rising compared to marine-terminating glacier runoff, TA concentrations of the freshwater endmember will possibly increase. This decreases pCO_2 in the surface waters (*Pilcher et al.*, 2018) and might counteract the effect of warm surface waters and upwelling, which promote an outgassing of CO_2 to the atmosphere. Thus, the ability of Scoresby Sund to be a CO_2 source will probably diminish.

II. However, basal ice of the GrIS contains a high concentration of dissolved CO_2. As soon as melting reaches those ice layers, this CO_2 will be transferred to ocean and atmosphere, and will further increase the partial pressure of CO_2 in both systems (*Ryu and Jacobson*, 2012).

III. Intensified meltwater plumes from submarine discharge will increase turbulence and upwelling in Nordvestfjord. Nonetheless, also the surface meltwater layer will thicken, which contains silts and has the potential to restrict primary production by shadowing and by sealing nutrients at depth. Primary production will therefore probably be more limited than nowadays, like proposed by (*Murray et al.*, 2015) for Godthåbsfjord and Young Sound.

IV. In Outer Scoresby Sund, a stronger buoyancy-driven circulation raises the import of nutrients from the shelf, similar to the projections for other Greenland fjords (*Rysgaard et al.*, 2003; *Arendt et al.*, 2010). The productivity of the Outer

Scoresby Sund might therefore be promoted with ongoing increase in meltwater discharge.

V. Ballasting by minerals in meltwater can further enhance sinking velocities and, hence, increase the burial of organic carbon at depth. This holds especially true for Nordvestfjord, where more meltwater drains into the system. Microbial degradation might, however, also be intensified due to the warmer water (*Iversen and Ploug*, 2013) and can therefore counteract the efficient export of particulate matter. Still, enhanced export has the ability fuel the benthic community (*Arendt et al.*, 2010).

VI. Not only the fjord water, but also the water at the shelf is freshening with increasing discharge from the GrIS. A shift towards fresher coastal water prevents the exchange of bottom water, as observed in Young Sound (*Boone*, 2018). In Scoresby Sund, this might result in a decreasing ventilation rate of the waters in Nordvestfjord's basin, impacting the carbon cycling in deep waters and at the sea floor.

More research is necessary to make more robust projections about the future fate of Greenland's fjords in general and Scoresby Sund in particular. As each fjord system has its own characteristics and concepts cannot easily be transferred from one to the other, research questions like which offshore oceanic changes are transmitted to the glacier fronts (*Carr et al.*, 2017) need to be analysed in more detail. Also, the continuous measurement of carbon system parameters, like TA and DIC (*Wanninkhof et al.*, 2013; *Fine et al.*, 2017), reveals important implications about the pathway anthropogenic CO_2 emissions may take and how our oceans are affected by this. Autonomous and moored platforms could facilitate this research in the future (reviewed by *McKinley et al.*, 2017). These measurements could then be used for modelling approaches, resulting in increasingly resolved forecasts for remote, but essential areas like Greenland's fjords.

Chapter 6

Appendix

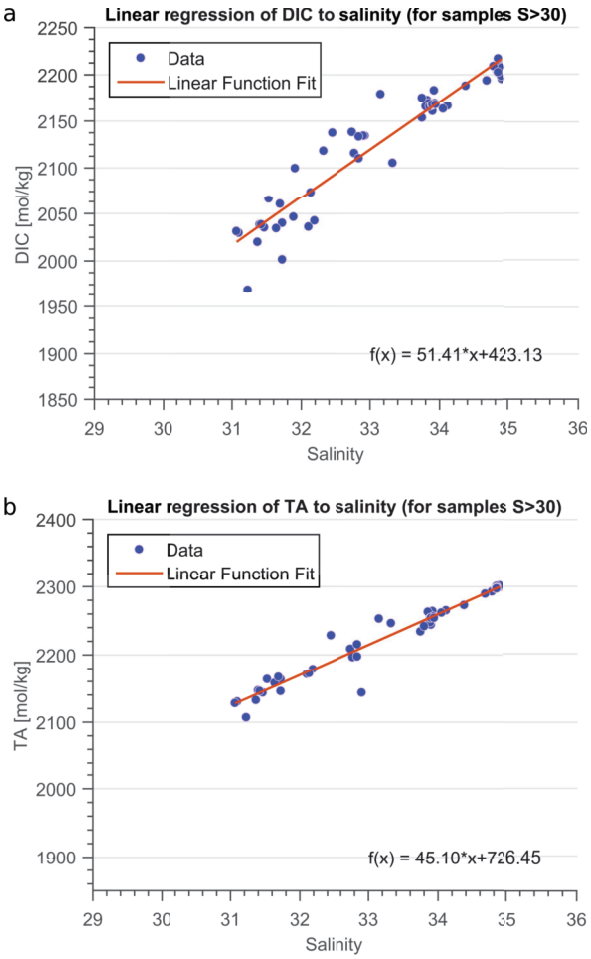

Figure A.1: (a) DIC and (b) TA correlated with salinity. Only samples with salinities >30 were included. R^2 for DIC is 0.906, for TA 0.942.

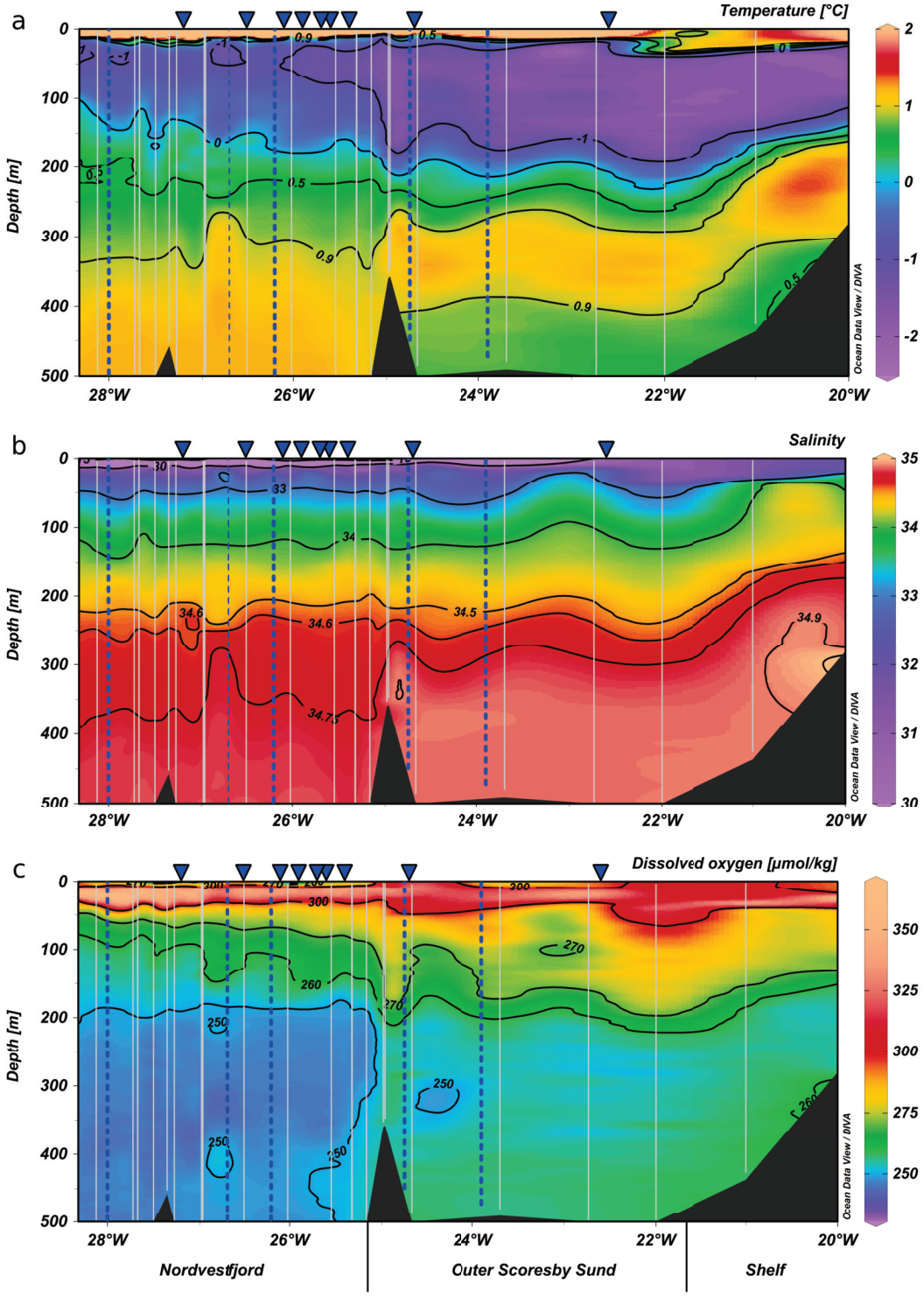

Figure A.2: (a) Temperature, (b) salinity, and (c) dissolved oxygen along the transect from the fjord head (left) to the fjord mouth (right) in the upper 500 m. Stations and sampling depths are indicated by white vertical lines. Blue vertical lines indicate the positions of marine-terminating glaciers, blue inverse triangles show the positions of surface meltwater inflow. Note that on the very left side (fjord head), the Daugaard-Jensen glacier calves into the fjord.

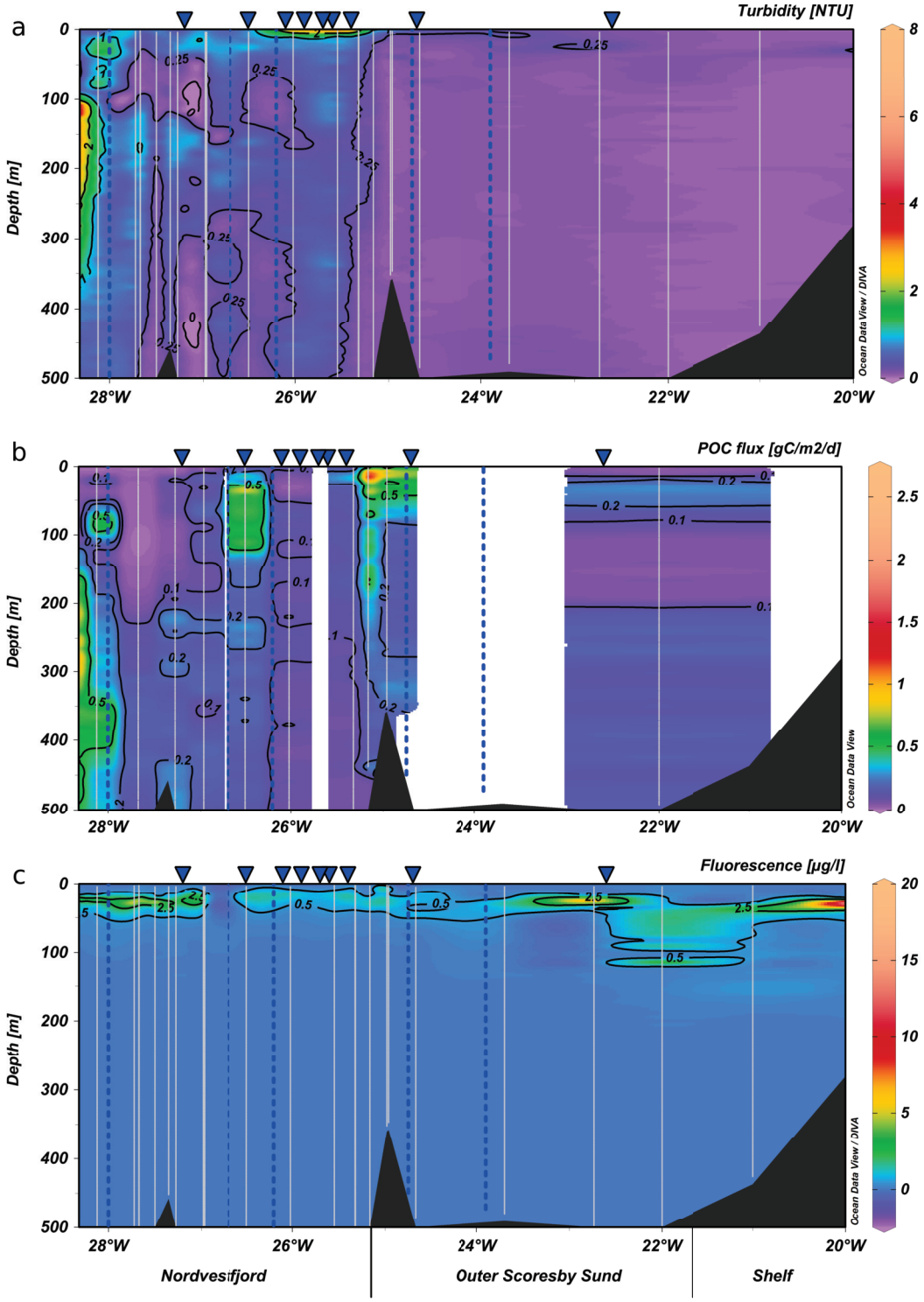

Figure A.3: (a) Turbidity, (b) flux of particulate organic carbon (POC), and (c) fluorescence along the transect from the fjord head (left) to the fjord mouth (right) in the upper 500 m. Labelling is similar to Fig. A.2.

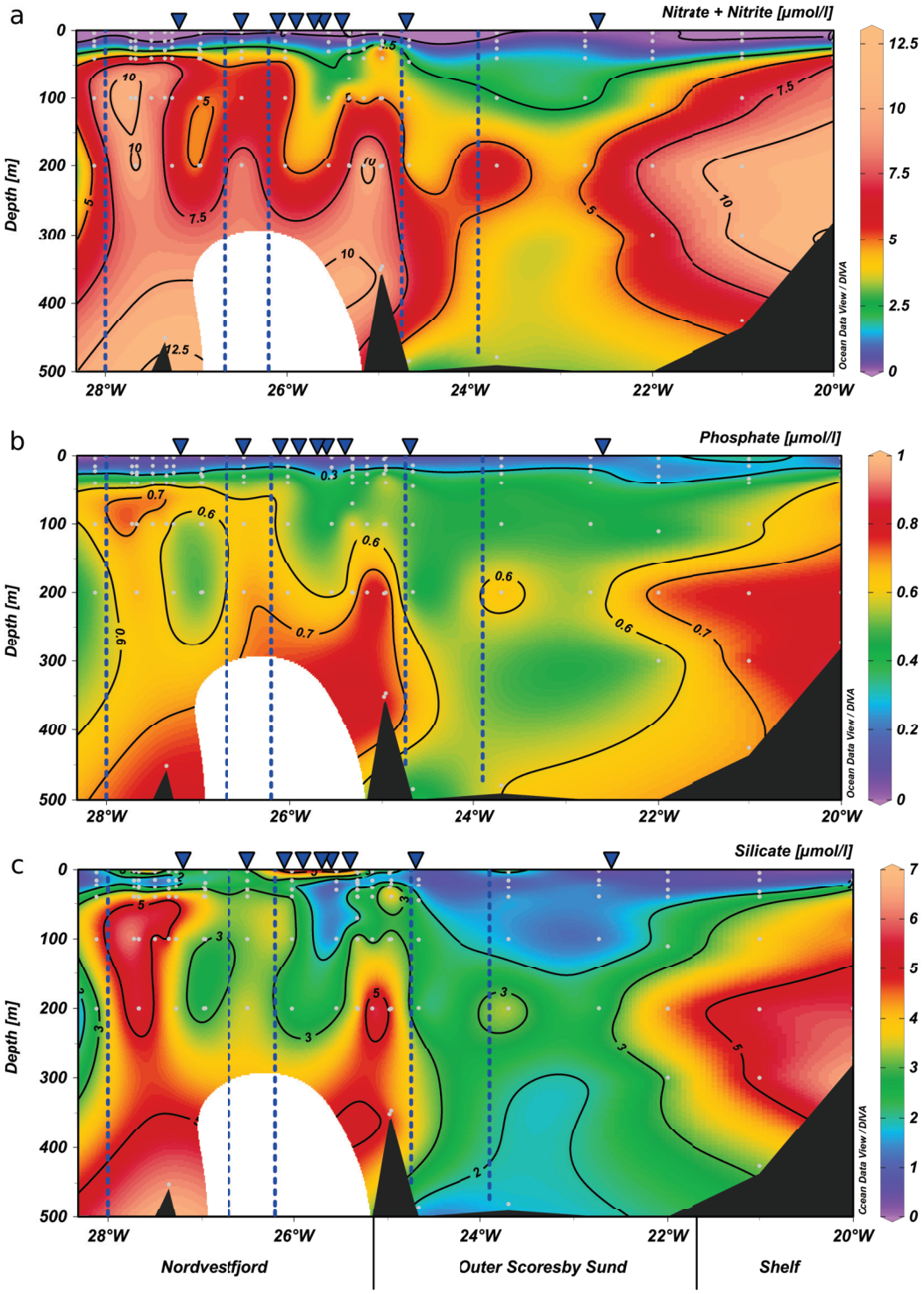

Figure A.4: Nutrient concentrations ((a) nitrate/nitrite, (b) phosphate, (c) silicate along the transect from the fjord head (left) to the fjord mouth (right) in the upper 500 m. Labelling is similar to Fig. A.2.

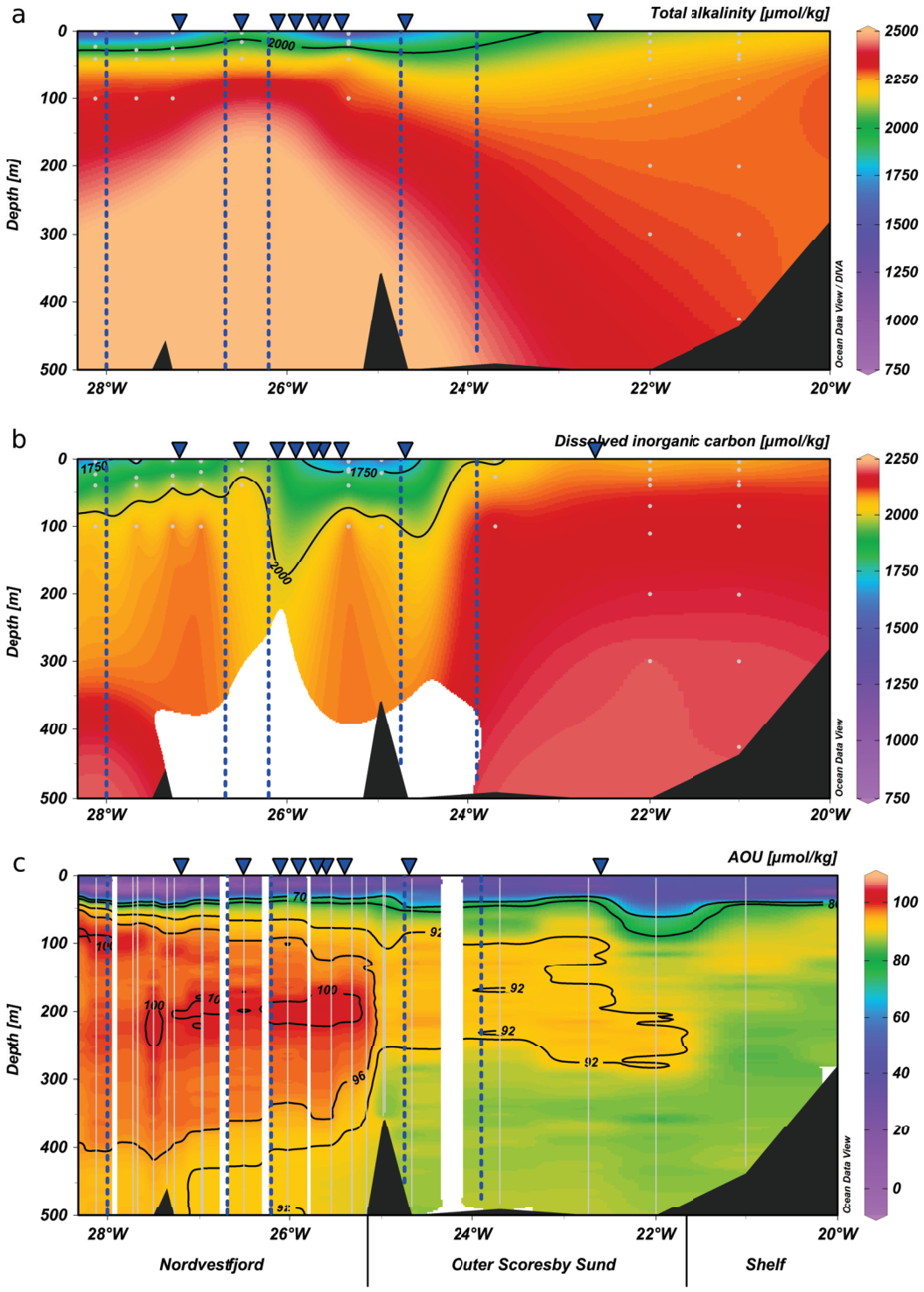

Figure A.5: (a) TA, (b) DIC, and (c) apparent oxygen utilization (AOU) along the transect from the fjord head (left) to the fjord mouth (right) in the upper 500 m. Labelling is similar to Fig. A.2.

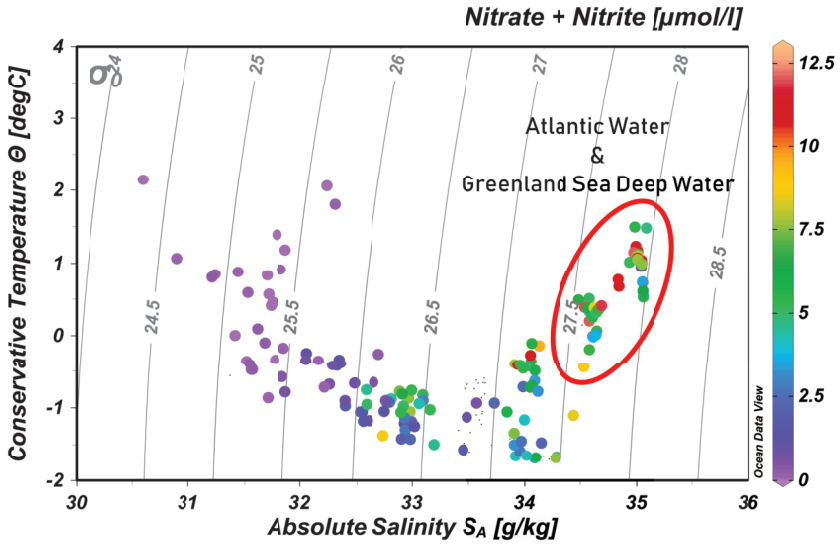

Figure A.6: T/S plot and related nitrate+nitrite concentrations, showing that mainly Atlantic Water and Greenland Sea Deep Water carry an elevated load of nutrients.

Bibliography

Alldredge, A. L., and K. M. Crocker (1995), Why do sinking mucilage aggregates accumulate in the water column?, *Sci. Total Environ.*, *165*, 15–22.

Alldredge, A. L., and M. W. Silver (1988), Characteristics, dynamics and significance of marine snow, *Prog. Oceanogr.*, *20*, 41–82.

Anderson, L. G., E. P. Jones, and J. H. Swift (2003), Export production in the central Arctic Ocean evaluated from phosphate deficits, *J. Geophys. Res.*, *108*(C6), 3199, doi:10.1029/2001JC001057.

Anderson, L. G., E. Falck, E. P. Jones, S. Jutterström, and J. H. Swift (2004), Enhanced uptake of atmospheric CO_2 during freezing of seawater: A field study in Storfjorden, Svalbard, *J. Geophys. Res.*, *109*, C06004, doi:10.1029/2003JC002120.

Andersson, A., E. Falck, A. Sjöblom, N. Kljun, E. Sahlée, A. M. Omar, and A. Rutgersson (2017), Air-sea gas transfer in high Arctic fjords, *Geophys. Res. Lett.*, *44*, 2519–2526.

Arendt, K. E., T. G. Nielsen, S. Rysgaard, and K. Tönnesson (2010), Differences in plankton community structure along the Godthåbsfjord, from the Greenland Ice Sheet to offshore waters, *Mar. Ecol. Prog. Ser.*, *401*, 49–62.

Arendt, K. E., M. D. Agersted, M. K. Sejr, and T. Juul-Pedersen (2016), Glacial meltwater influences on plankton community structure and the importance of top-down control (of primary production) in a NE Greenland fjord, *Estuarine Coastal Shelf Sci.*, *183*, 123–135.

Bacon, S., G. Reverdin, I. G. Rigor, and H. M. Snaith (2002), A freshwater jet on the east Greenland shelf, *J. Geophys. Res.-Oceans*, *107*(C7), 3068, doi:10.1029/2001JC000935.

Bamber, J. L., J. A. Griggs, R. T. W. L. Hurkmans, J. A. Dowdeswell, S. P. Gogineni, I. Howat, J. Mouginot, J. Paden, S. Palmer, E. Rignot, et al. (2013), A new bed elevation dataset for Greenland, *Cryosphere*, *7*, 499–510.

Bates, N. R., M. H. P. Best, and D. A. Hansell (2005), Spatio-temporal distribution of dissolved inorganic carbon and net community production in the Chukchi and Beaufort Seas, *Deep Sea Res. Part II*, *52*, 3303 – 3323.

Bates, N. R., S. B. Moran, D. A. Hansell, and J. T. Mathis (2006), An increasing CO_2 sink in the Arctic Ocean due to sea-ice loss, *Geophys. Res. Lett.*, *33*, L23609, doi:10.1029/2006GL027028.

Bates, N. R., R. Garley, K. E. Frey, K. L. Shake, and J. T. Mathis (2014), Sea-ice melt CO_2-carbonate chemistry in the western Arctic Ocean: meltwater contributions to air-sea CO_2 gas exchange, mixed-layer properties and rates of net community production under sea ice, *Biogeosciences*, *11*, 6769–6789.

Beaton, A. D., J. L. Wadham, J. Hawkings, E. A. Bagshaw, G. Lamarche-Gagnon, M. C. Mowlem, and M. Tranter (2017), High-resolution in situ measurement of nitrate in runoff from the Greenland Ice Sheet, *Environ. Sci. Technol.*, *51*, 12518–12527.

Belcher, A., M. Iversen, C. Manno, S. A. Henson, G. A. Tarling, and R. Sanders (2016), The role of particle associated microbes in remineralization of fecal pellets in the upper mesopelagic of the Scotia Sea, Antarctica, *Limnol. Oceanogr.*, *61*, 1049–1064.

Bendtsen, J., J. Mortensen, and S. Rysgaard (2015), Modelling subglacial discharge and its influence on ocean heat transport in Arctic fjords, *Ocean Dyn.*, *65*, 1535–1546.

Boone, W. (2018), Seasonal and interannual variability of oceanographic conditions in a Northeast Greenland Fjord, Ph.D. thesis, University of Manitoba.

Boyd, P. W., and T. W. Trull (2007), Understanding the export of biogenic particles in oceanic waters: Is there consensus?, *Prog. Oceanogr.*, *72*, 276–312.

Brewer, P. G., and J. C. Goldman (1976), Alkalinity changes generated by phytoplankton growth, *Limnol. Oceanogr.*, *21*(1), 108–117.

Brown, G. H. (2002), Glacier meltwater hydrochemistry, *Appl. Geochem.*, *17*, 855–883.

Burgers, T. M., L. A. Miller, H. Thomas, B. G. T. Else, M. Gosselin, and T. Papakyriakou (2017), Surface water pCO_2 variations and sea-air CO_2 fluxes during summer in the Eastern Canadian Arctic, *J. Geophys. Res.-Oceans*, *122*, doi: 10.1002/2017JC013250.

Cai, W.-J., L. Chen, B. Chen, Z. Gao, S. H. Lee, J. Chen, D. Pierrot, K. Sullivan, Y. Wang, X. Hu, W.-J. Huang, Y. Zhang, S. Xu, A. Murata, J. M. Grebmeier, E. P. Jones, and H. Zhang (2010), Decrease in the CO_2 uptake capacity in an ice-free Arctic Ocean basin, *Science*, *329*(5991), 556–559.

Carr, J. R., C. R. Stokes, and A. Vieli (2017), Threefold increase in marine-terminating outlet glacier retreat rates across the Atlantic Arctic: 1992–2010, *Ann. Glaciol.*, *58*(74), 72–91.

Cofaigh, C. Ó., J. A. Dowdeswell, and H. Grobe (2001), Holocene glacimarine sedimentation, inner Scoresby Sund, East Greenland: the influence of fast-flowing ice-sheet outlet glaciers, *Mar. Geol.*, *175*, 103–129.

Cowton, T., A. Sole, P. Nienow, D. Slater, D. Wilton, and E. Hanna (2016), Controls on the transport of oceanic heat to Kangerdlugssuaq Glacier, East Greenland, *J. Glaciol.*, *62*(236), 1167–1180.

Cross, J. N., J. T. Mathis, N. R. Bates, and R. H. Byrne (2013), Conservative and non-conservative variations of total alkalinity on the southeastern Bering Sea shelf, *Mar. Chem.*, *154*, 100–112.

Dickson, A. G., C. L. Sabine, and J. R. Christian (Eds.) (2007), Guide to Best Practices for Ocean CO_2 Measurements, *PICES Spec. Publ.*, *3*, 191 pp.

Dowdeswell, J. A., H. Villinger, R. J. Whittington, and P. Marienfeld (1993), Iceberg scouring in Scoresby Sund and on the East Greenland continental shelf, *Mar. Geol.*, *111*, 37–53.

Dowdeswell, J. A., C. L. Batchelor, K. A. Hogan, and H.-W. Schenke (2016), Nordvestfjord: a major East Greenland fjord system, in *Atlas of Submarine Glacial Landforms: Modern, Quaternary and Ancient, Geological Society, London, Memoirs*, vol. 46, edited by J. A. Dowdeswell, M. Canals, M. Jakobsson, B. J. Todd, E. K. Dowdeswell, and K. A. Hogan, pp. 43–44.

Enderlin, E. M., and I. M. Howat (2013), Submarine melt rate estimates for floating termini of Greenland outlet glaciers (2000–2010), *J. Glaciol.*, *59*(213), 67–75.

Enderlin, E. M., G. S. Hamilton, F. Straneo, and D. A. Sutherland (2016), Iceberg meltwater fluxes dominate the freshwater budget in Greenland's iceberg-congested glacial fjords, *Geophys. Res. Lett.*, *43*, 11,287–11,294, doi:10.1002/2016GL070718.

Findlay, H. S., G. Gibson, M. Kędra, N. Morata, M. Orchowska, A. K. Pavlov, M. Reigstad, A. Silyakova, J.-É. Tremblay, W. Walczowski, et al. (2015), Responses in Arctic marine carbon cycle processes: conceptual scenarios and implications for ecosystem function, *Polar Res.*, *34*(1), 24252, doi:10.3402/polar.v34.24252.

Fine, R. A., D. A. Willey, and F. J. Millero (2017), Global variability and changes in ocean total alkalinity from Aquarius satellite data, *Geophys. Res. Lett.*, *44*, 261–267.

Francois, R., S. Honjo, R. Krishfield, and S. Manganini (2002), Factors controlling the flux of organic carbon to the bathypelagic zone of the ocean, *Global Biogeochem. Cycles*, *16*(4), 1087, doi:10.1029/2001GB001722.

Fransson, A., M. Chierici, L. A. Miller, G. Carnat, E. Shadwick, H. Thomas, S. Pineault, and T. N. Papakyriakou (2013), Impact of sea-ice processes on the carbonate system and ocean acidification at the ice-water interface of the Amundsen Gulf, Arctic Ocean, *J. Geophys. Res.-Oceans*, *118*, 7001–7023.

Fried, M. J., G. A. Catania, T. C. Bartholomaus, D. Duncan, M. Davis, L. A. Stearns, J. Nash, E. Shroyer, and D. Sutherland (2015), Distributed subglacial discharge drives significant submarine melt at a Greenland tidewater glacier, *Geophys. Res. Lett.*, *42*, 9328–9336.

Friis, K., A. Körtzinger, and D. W. R. Wallace (2003), The salinity normalization of marine inorganic carbon chemistry data, *Geophys. Res. Lett.*, *30*(2), 1085, doi: 10.1029/2002GL015898.

Funder, S. (1972), Deglaciation of the Scoresby Sund fjord region, north-east Greenland, *Fr. Bagges Kgl. Hofbogtrykkeri*, *4*, 33–42.

Glud, R. N., and S. Rysgaard (2007), The annual organic carbon budget of Young Sound, NE Greenland, in *Carbon Cycling in Arctic marine ecosystems: Case study Young Sound, Meddr. Grønland, Bioscience, 58*, edited by S. Rysgaard and R. N. Glud, pp. 194–203.

Glud, R. N., M. Kühl, F. Wenzhöfer, and S. Rysgaard (2002), Benthic diatoms of a high Arctic fjord (Young Sound, NE Greenland): importance for ecosystem primary production, *Mar. Ecol. Prog. Ser.*, *238*, 15–29.

Gran, G. (1952), Determination of the equivalence point in potentiometric titrations. Part II, *Analyst*, *77*, 661–671.

Guidi, L., G. A. Jackson, L. Stemmann, J. C. Miquel, M. Picheral, and G. Gorsky (2008), Relationship between particle size distribution and flux in the mesopelagic zone, *Deep Sea Res. Part I*, *55*, 1364–1374.

Guidi, L., L. Legendre, G. Reygondeau, J. Uitz, L. Stemmann, and S. A. Henson (2015), A new look at ocean carbon remineralization for estimating deepwater sequestration, *Global Biogeochem. Cycles*, *29*, 1044–1059.

Hansell, D. A., and C. A. Carlson (1998), Net community production of dissolved organic carbon, *Global Biogeochem. Cycles*, *12*(3), 443–453.

Harrison, W. G., and G. F. Cota (1991), Primary production in polar waters: relation to nutrient availability, *Polar Res.*, *10*(1), 87–104.

Hartman, S. E., C. Dumousseaud, and A. Roberts (2011), Operating manual for the Marianda (Versatile Instrument for the determination of Titration Alkalinity) VINDTA 3c for the laboratory based determination of Total Alkalinity and Total Dissolved Inorganic Carbon in seawater, *National Oceanography Centre Internal Document, No. 01, Southhampton, UK (Unpublished manuscript)*, 66 pp.

Håvik, L., R. S. Pickart, K. Våge, D. Torres, A. M. Thurnherr, A. Beszczynska-Möller, W. Walczowski, and W.-J. von Appen (2017), Evolution of the East Greenland Current from Fram Strait to Denmark Strait: Synoptic measurements from summer 2012, *J. Geophys. Res.-Oceans*, *122*, 1974–1994.

Hawkings, J., J. Wadham, M. Tranter, J. Telling, E. Bagshaw, A. Beaton, S.-L. Simmons, D. Chandler, A. Tedstone, and P. Nienow (2016), The Greenland Ice Sheet as a hot spot of phosphorus weathering and export in the Arctic, *Global Biogeochem. Cycles*, *30*, 191–210.

Hawkings, J. R., J. L. Wadham, M. Tranter, E. Lawson, A. Sole, T. Cowton, A. J. Tedstone, I. Bartholomew, P. Nienow, D. Chandler, et al. (2015), The effect of warming climate on nutrient and solute export from the Greenland Ice Sheet, *Geochem. Persp. Lett.*, *1*, 94–104.

Hawkings, J. R., J. L. Wadham, L. G. Benning, K. R. Hendry, M. Tranter, A. Tedstone, P. Nienow, and R. Raiswell (2017), Ice sheets as a missing source of silica to the polar oceans, *Nat. Commun.*, *8*, 14198, doi:10.1038/ncomms14198.

Hoppema, M., L. Goeyens, and E. Fahrbach (2000), Intense nutrient removal in the remote area off Larsen Ice Shelf (Weddell Sea), *Polar Biol.*, *23*, 85–94.

Hoppema, M., R. Middag, H. J. W. de Baar, E. Fahrbach, E. M. van Weerlee, and H. Thomas (2007), Whole season net community production in the Weddell Sea, *Polar Biol.*, *31*, 101–111.

Hopwood, M. J., D. P. Connelly, K. E. Arendt, T. Juul-Pedersen, M. C. Stinchcombe, L. Meire, M. Esposito, and R. Krishna (2016), Seasonal changes in Fe along a glaciated Greenlandic fjord, *Front. Earth Sci.*, *4*(15), doi:10.3389/feart.2016.00015.

Hudson, B., I. Overeem, D. McGrath, J. P. M. Syvitski, A. Mikkelsen, and B. Hasholt (2014), MODIS observed increase in duration and spatial extent of sediment plumes in Greenland fjords, *Cryosphere*, *8*, 1161–1176.

IPCC (2014), *Climate Change 2014: Synthesis Report. Contribution of Working Groups I, II and III to the Fifth Assessment Report of the Intergovernmental Panel on Climate Change*, IPCC, Geneva, Switzerland, 151 pp.

Iversen, M. H., and H. Ploug (2013), Temperature effects on carbon-specific respiration rate and sinking velocity of diatom aggregates – potential implications for deep ocean export processes, *Biogeosciences*, *10*, 4073–4085.

Iversen, M. H., and M. L. Robert (2015), Ballasting effects of smectite on aggregate formation and export from a natural plankton community, *Mar. Chem.*, *175*, 18–27.

Iversen, M. H., N. Nowald, H. Ploug, G. A. Jackson, and G. Fischer (2010), High resolution profiles of vertical particulate organic matter export off Cape Blanc, Mauritania: Degradation processes and ballasting effects, *Deep Sea Res. Part I*, *57*, 771–784.

Jackson, G. A., and A. B. Burd (2015), Simulating aggregate dynamics in ocean biogeochemical models, *Prog. Oceanogr.*, *133*, 55–65.

Jackson, R. H., and F. Straneo (2016), Heat, salt, and freshwater budgets for a glacial fjord in Greenland, *J. Phys. Oceanogr.*, *46*, 2735–2768.

Jackson, R. H., F. Straneo, and D. A. Sutherland (2014), Externally forced fluctuations in ocean temperature at Greenland glaciers in non-summer months, *Nat. Geosci.*, *7*, 503–508.

Jennings Jr, J. C., L. I. Gordon, and D. M. Nelson (1984), Nutrient depletion indicates high primary productivity in the Weddell Sea, *Nature*, *309*, 51–54.

Johnson, K. M., K. D. Wills, D. B. Butler, W. K. Johnson, and C. S. Wong (1993), Coulometric total carbon dioxide analysis for marine studies: maximizing the performance of an automated gas extraction system and coulometric detector, *Mar. Chem.*, *44*, 167–187.

Jones, E. M., D. C. E. Bakker, H. J. Venables, M. J. Whitehouse, R. E. Korb, and A. J. Watson (2010), Rapid changes in surface water carbonate chemistry during Antarctic sea ice melt, *Tellus B*, *62*(5), 621–635.

Juul-Pedersen, T., K. E. Arendt, J. Mortensen, M. E. Blicher, D. H. Søgaard, and S. Rysgaard (2015), Seasonal and interannual phytoplankton production in a sub-Arctic tidewater outlet glacier fjord, SW Greenland, *Mar. Ecol. Prog. Ser.*, *524*, 27–38.

Karakaş, G., N. Nowald, C. Schäfer-Neth, M. Iversen, W. Barkmann, G. Fischer, P. Marchesiello, and R. Schlitzer (2009), Impact of particle aggregation on vertical fluxes of organic matter, *Prog. Oceanogr.*, *83*, 331–341.

Kattner, G., and H. Becker (1991), Nutrients and organic nitrogenous compounds in the marginal ice zone of the Fram Strait, *J. Mar. Syst.*, *2*, 385–394.

Khan, S. A., K. H. Kjær, M. Bevis, J. L. Bamber, J. Wahr, K. K. Kjeldsen, A. A. Bjørk, N. J. Korsgaard, L. A. Stearns, M. R. van den Broeke, et al. (2014), Sustained mass loss of the northeast Greenland ice sheet triggered by regional warming, *Nat. Clim. Change*, *4*, 292–299.

Lalande, C., B. Moriceau, A. Leynaert, and N. Morata (2016), Spatial and temporal variability in export fluxes of biogenic matter in Kongsfjorden, *Polar Biol.*, *39*, 1725–1738.

Lauderdale, J. M., S. Dutkiewicz, R. G. Williams, and M. J. Follows (2016), Quantifying the drivers of ocean-atmosphere CO_2 fluxes, *Global Biogeochem. Cycles*, *30*, 983–999.

Lee, K. (2001), Global net community production estimated from the annual cycle of surface water total dissolved inorganic carbon, *Limnol. Oceanogr.*, *46*(6), 1287–1297.

Li, W. K. W., F. A. McLaughlin, C. Lovejoy, and E. C. Carmack (2009), Smallest algae thrive as the Arctic Ocean freshens, *Science*, *326*(5952), 539.

Martin, J. H., G. A. Knauer, D. M. Karl, and W. W. Broenkow (1987), VERTEX: carbon cycling in the northeast Pacific, *Deep Sea Res.*, *34*(2), 267–285.

Mathis, J. T., N. R. Bates, D. A. Hansell, and T. Babila (2009), Net community production in the northeastern Chukchi Sea, *Deep Sea Res. Part II*, *56*, 1213–1222.

Mathis, J. T., J. N. Cross, N. R. Bates, S. Bradley Moran, M. W. Lomas, C. W. Mordy, and P. J. Stabeno (2010), Seasonal distribution of dissolved inorganic carbon and net community production on the Bering Sea shelf, *Biogeosciences*, *7*, 1769–1787.

Mathis, J. T., R. S. Pickart, R. H. Byrne, C. L. McNeil, G. W. K. Moore, L. W. Juranek, X. Liu, J. Ma, R. A. Easley, M. M. Elliot, et al. (2012), Storm-induced upwelling of high pCO_2 waters onto the continental shelf of the western Arctic Ocean and implications for carbonate mineral saturation states, *Geophys. Res. Lett.*, *39*, L07606, doi:10.1029/2012GL051574.

McKinley, G. A., A. R. Fay, N. S. Lovenduski, and D. J. Pilcher (2017), Natural variability and anthropogenic trends in the ocean carbon sink, *Annu. Rev. Mar. Sci.*, *9*, 125–150.

McMahon, T. G., and J. W. Patching (1984), Fluxes of organic carbon in a fjord on the west coast of Ireland, *Estuarine Coastal Shelf Sci.*, *19*, 205–215.

Meire, L., D. H. Søgaard, J. Mortensen, F. J. R. Meysman, K. Soetaert, K. E. Arendt, T. Juul-Pedersen, M. E. Blicher, and S. Rysgaard (2015), Glacial meltwater and primary production are drivers of strong CO_2 uptake in fjord and coastal waters adjacent to the Greenland Ice Sheet, *Biogeosciences*, *12*, 2347–2363.

Meire, L., P. Meire, E. Struyf, D. W. Krawczyk, K. E. Arendt, J. C. Yde, T. Juul Pedersen, M. J. Hopwood, S. Rysgaard, and F. J. R. Meysman (2016a), High export of dissolved silica from the Greenland Ice Sheet, *Geophys. Res. Lett.*, *43*, 9173–9182.

Meire, L., J. Mortensen, S. Rysgaard, J. Bendtsen, W. Boone, P. Meire, and F. J. R. Meysman (2016b), Spring bloom dynamics in a subarctic fjord influenced by tidewater outlet glaciers (Godthåbsfjord, SW Greenland), *J. Geophys. Res.-Biogeosci.*, *121*, 1581–1592.

Meire, L., J. Mortensen, P. Meire, T. Juul-Pedersen, M. K. Sejr, S. Rysgaard, R. Nygaard, P. Huybrechts, and F. J. R. Meysman (2017), Marine-terminating glaciers sustain high productivity in Greenland fjords, *Global Change Biol.*, *23*, 5344–5357.

Middelbo, A. B., M. K. Sejr, K. E. Arendt, and E. F. Møller (2018), Impact of glacial meltwater on spatiotemporal distribution of copepods and their grazing impact in Young Sound NE, Greenland, *Limnol. Oceanogr.*, *63*, 322–336.

Mintrop, L., F. F. Pérez, M. González Dávila, J. M. Santana Casiano, and A. Körtzinger (2000), Alkalinity determination by potentiometry: intercalibration using three different methods, *Ciencias Marinas*, *26*(1), 23–27.

Mook, W. G., and B. K. S. Koene (1975), Chemistry of dissolved inorganic carbon in estuarine and coastal brackish waters, *Estuarine Coastal Mar. Sci.*, *3*, 325–336.

Moon, T., D. A. Sutherland, D. Carroll, D. Felikson, L. Kehrl, and F. Straneo (2017), Subsurface iceberg melt key to Greenland fjord freshwater budget, *Nat. Geosci.*, *11*, 49–54.

Mortensen, J., K. Lennert, J. Bendtsen, and S. Rysgaard (2011), Heat sources for glacial melt in a sub-arctic fjord (Godthåbsfjord) in contact with the Greenland Ice Sheet, *J. Geophys. Res.-Oceans*, *116*, C01013, doi:10.1029/2010JC006528.

Mugford, R. I., and J. A. Dowdeswell (2011), Modeling glacial meltwater plume dynamics and sedimentation in high-latitude fjords, *J. Geophys. Res.*, *116*, F01023, doi:10.1029/2010JF001735.

Munro, D. R., N. S. Lovenduski, B. B. Stephens, T. Newberger, K. R. Arrigo, T. Takahashi, P. D. Quay, J. Sprintall, N. M. Freeman, and C. Sweeney (2015), Estimates of net community production in the Southern Ocean determined from time series

observations (2002–2011) of nutrients, dissolved inorganic carbon, and surface ocean pCO_2 in Drake Passage, *Deep Sea Res. Part II*, *114*, 49–63.

Murray, C., S. Markager, C. A. Stedmon, T. Juul-Pedersen, M. K. Sejr, and A. Bruhn (2015), The influence of glacial melt water on bio-optical properties in two contrasting Greenlandic fjords, *Estuarine Coastal Shelf Sci.*, *163*, 72–83.

Nienow, P. W., A. J. Sole, D. A. Slater, and T. R. Cowton (2017), Recent advances in our understanding of the role of meltwater in the Greenland Ice Sheet system, *Curr. Clim. Change Rep.*, *3*, 330–344.

Notz, D., and J. Stroeve (2016), Observed Arctic sea-ice loss directly follows anthropogenic CO_2 emission, *Science*, *354*(6313), 747–750.

Nowald, N., G. Fischer, V. Ratmeyer, M. Iversen, C. Reuter, and G. Wefer (2009), In-situ sinking speed measurements of marine snow aggregates acquired with a settling chamber mounted to the Cherokee ROV, in *Oceans 2009-Europe*, pp. 1–6, IEEE.

Passow, U., and C. L. De La Rocha (2006), Accumulation of mineral ballast on organic aggregates, *Global Biogeochem. Cycles*, *20*, GB1013, doi:10.1029/2005GB002579.

Petrik, C. M., G. A. Jackson, and D. M. Checkley Jr (2013), Aggregates and their distributions determined from LOPC observations made using an autonomous profiling float, *Deep Sea Res. Part I*, *74*, 64–81.

Pilcher, D. J., S. A. Siedlecki, A. J. Hermann, K. O. Coyle, J. T. Mathis, and W. Evans (2018), Simulated impact of glacial runoff on CO_2 uptake in the Gulf of Alaska, *Geophys. Res. Lett.*, *45*, 880–890.

Ploug, H., M. H. Iversen, M. Koski, and E. T. Buitenhuis (2008), Production, oxygen respiration rates, and sinking velocity of copepod fecal pellets: Direct measurements of ballasting by opal and calcite, *Limnol. Oceanogr.*, *53*(2), 469–476.

Poulsen, L. K., and M. H. Iversen (2008), Degradation of copepod fecal pellets: key role of protozooplankton, *Mar. Ecol. Prog. Ser.*, *367*(1–13), doi:10.3354/meps07611.

Reisdorph, S. C., and J. T. Mathis (2014), The dynamic controls on carbonate mineral saturation states and ocean acidification in a glacially dominated estuary, *Estuarine Coastal Shelf Sci.*, *144*, 8–18.

Reisdorph, S. C., and J. T. Mathis (2015), Assessing net community production in a glaciated Alaskan fjord, *Biogeosciences*, *12*, 5185–5198.

Rignot, E., and P. Kanagaratnam (2006), Changes in the velocity structure of the Greenland Ice Sheet, *Science*, *311*, 986–990.

Rudels, B., L. G. Anderson, and E. P. Jones (1996), Formation and evolution of the surface mixed layer and halocline of the Arctic Ocean, *J. Geophys. Res.*, *101*(C4), 8807–8821.

Rüggeberg, A., S. Flögel, W.-C. Dullo, K. Hissmann, and A. Freiwald (2011), Water mass characteristics and sill dynamics in a subpolar cold-water coral reef setting at Stjernsund, northern Norway, *Mar. Geol.*, *282*, 5–12.

Rutgers van der Loeff, M. M., N. Cassar, M. Nicolaus, B. Rabe, and I. Stimac (2014), The influence of sea ice cover on air-sea gas exchange estimated with radon-222 profiles, *J. Geophys. Res.-Oceans*, *119*, 2735–2751.

Rysgaard, S., and R. N. Glud (2007), Carbon cycling and climate change: Predictions for a high Arctic marine ecosystem (Young Sound, NE Greenland), in *Carbon Cycling in Arctic marine ecosystems: Case study Young Sound, Meddr. Grønland, Bioscience, 58*, edited by S. Rysgaard and R. N. Glud, pp. 206–214.

Rysgaard, S., and T. G. Nielsen (2006), Carbon cycling in a high-arctic marine ecosystem – Young Sound, NE Greenland, *Prog. Oceanogr.*, *71*, 426–445.

Rysgaard, S., B. Thamdrup, N. Risgaard-Petersen, H. Fossing, P. Berg, P. B. Christensen, and T. Dalsgaard (1998), Seasonal carbon and nutrient mineralization in a high-Arctic coastal marine sediment, Young Sound, Northeast Greenland, *Mar. Ecol. Prog. Ser.*, *175*, 261–276.

Rysgaard, S., T. Vang, M. Stjernholm, B. Rasmussen, A. Windelin, and S. Kiilsholm (2003), Physical conditions, carbon transport, and climate change impacts in a northeast Greenland fjord, *Arct. Antarct. Alp. Res.*, *35*(3), 301–312.

Rysgaard, S., J. Bendtsen, L. T. Pedersen, H. Ramløv, and R. N. Glud (2009), Increased CO_2 uptake due to sea ice growth and decay in the Nordic Seas, *J. Geophys. Res.*, *114*, C09011, doi:10.1029/2008JC005088.

Rysgaard, S., J. Mortensen, T. Juul-Pedersen, L. L. Sørensen, K. Lennert, D. H. Søgaard, K. E. Arendt, M. E. Blicher, M. K. Sejr, and J. Bendtsen (2012), High air–sea CO_2 uptake rates in nearshore and shelf areas of Southern Greenland: Temporal and spatial variability, *Mar. Chem.*, *128-129*, 26–33.

Rysgaard, S., J. Bendtsen, J. Mortensen, and M. K. Sejr (2018), High geothermal heat flux in close proximity to the Northeast Greenland Ice Stream, *Sci. Rep.*, *8*(1344), doi:10.1038/s41598-018-19244-x.

Ryu, J.-S., and A. D. Jacobson (2012), CO_2 evasion from the Greenland Ice Sheet: A new carbon-climate feedback, *Chem. Geol.*, *320-321*, 80–95.

Schaffer, J., W.-J. von Appen, P. A. Dodd, C. Hofstede, C. Mayer, L. de Steur, and T. Kanzow (2017), Warm water pathways toward Nioghalvfjerdsfjorden Glacier, Northeast Greenland, *J. Geophys. Res.-Oceans*, *122*, 4004–4020.

Sciascia, R., F. Straneo, C. Cenedese, and P. Heimbach (2013), Seasonal variability of submarine melt rate and circulation in an East Greenland fjord, *J. Geophys. Res.-Oceans*, *118*, 2492–2506.

Sejr, M. K., D. Krause-Jensen, S. Rysgaard, L. L. Sørensen, P. B. Christensen, and R. N. Glud (2011), Air-sea flux of CO_2 in arctic coastal waters influenced by glacial melt water and sea ice, *Tellus B*, *63*(5), 815–822.

Sejr, M. K., C. A. Stedmon, J. Bendtsen, J. Abermann, T. Juul-Pedersen, J. Mortensen, and S. Rysgaard (2017), Evidence of local and regional freshening of Northeast Greenland coastal waters, *Scientific reports*, *7*(13183), doi:10.1038/s41598-017-10610-9.

Silyakova, A., R. G. J. Bellerby, K. G. Schulz, J. Czerny, T. Tanaka, G. Nondal, U. Riebesell, A. Engel, T. De Lange, and A. Ludvig (2013), Pelagic community production and carbon-nutrient stoichiometry under variable ocean acidification in an Arctic fjord, *Biogeosciences*, *10*, 4847–4859.

Smith, R. W., T. S. Bianchi, M. Allison, C. Savage, and V. Galy (2015), High rates of organic carbon burial in fjord sediments globally, *Nat. Geosci.*, *8*, 450–453.

Sørensen, H. L., L. Meire, T. Juul-Pedersen, H. C. de Stigter, F. J. R. Meysman, S. Rysgaard, B. Thamdrup, and R. N. Glud (2015), Seasonal carbon cycling in a Greenlandic fjord: an integrated pelagic and benthic study, *Mar. Ecol. Prog. Ser.*, *539*, 1–17.

Stevens, L. A., F. Straneo, S. B. Das, A. J. Plueddemann, A. L. Kukulya, and M. Morlighem (2016), Linking glacially modified waters to catchment-scale subglacial discharge using autonomous underwater vehicle observations, *Cryosphere*, *10*, 417–432.

Straneo, F. (2017), Glacier/ocean interactions in Greenland and their impact on the climate system, *Low Temperature Science*, *75*, 67–75.

Straneo, F., and C. Cenedese (2015), The dynamics of Greenland's glacial fjords and their role in climate, *Annu. Rev. Mar. Sci.*, *7*, 89–112.

Straneo, F., and P. Heimbach (2013), North Atlantic warming and the retreat of Greenland's outlet glaciers, *Nature*, *504*, 36–42.

Takahashi, T., S. C. Sutherland, R. Wanninkhof, C. Sweeney, R. A. Feely, D. W. Chipman, B. Hales, G. Friederich, F. Chavez, C. Sabine, et al. (2009), Climatological mean and decadal change in surface ocean pCO_2, and net sea–air CO_2 flux over the global oceans, *Deep Sea Res. Part II*, *56*, 554–577.

Tamelander, T., A. B. Aubert, and C. Wexels Riser (2012), Export stoichiometry and contribution of copepod faecal pellets to vertical flux of particulate organic carbon, nitrogen and phosphorus, *Mar. Ecol. Prog. Ser.*, *459*, 17–28.

Turner, J. T. (2015), Zooplankton fecal pellets, marine snow, phytodetritus and the ocean's biological pump, *Prog. Oceanogr.*, *130*, 205–248.

Ulfsbo, A., N. Cassar, M. Korhonen, S. van Heuven, M. Hoppema, G. Kattner, and L. G. Anderson (2014), Late summer net community production in the central Arctic Ocean using multiple approaches, *Global Biogeochem. Cycles*, *28*, 1129–1148.

Wadham, J. L., J. Hawkings, J. Telling, D. Chandler, J. Alcock, E. O'Donnell, P. Kaur, E. Bagshaw, M. Tranter, A. Tedstone, et al. (2016), Sources, cycling and export of nitrogen on the Greenland Ice Sheet, *Biogeosciences*, *13*, 6339–6352.

Walsh, K. M., I. M. Howat, Y. Ahn, and E. M. Enderlin (2012), Changes in the marine-terminating glaciers of central east Greenland, 2000–2010, *Cryosphere*, *6*, 211–220.

Wanninkhof, R., G.-H. Park, T. Takahashi, R. A. Feely, J. L. Bullister, and S. C. Doney (2013), Changes in deep-water CO_2 concentrations over the last several decades determined from discrete pCO_2 measurements, *Deep Sea Res. Part I*, *74*, 48–63.

Węsławski, J. M., and J. Legeżyńska (1998), Glaciers caused zooplankton mortality?, *J. Plankton Res.*, *20*(7), 1233–1240.

Wiedmann, I., M. Reigstad, M. Marquardt, A. Vader, and T. M. Gabrielsen (2016), Seasonality of vertical flux and sinking particle characteristics in an ice-free high arctic fjord—Different from subarctic fjords?, *J. Mar. Syst.*, *154*, 192–205.

Williams, P. J. I. (1993), On the definition of plankton production terms, *ICES mar. Sci. Symp.*, *197*, 9–19.

Wolf-Gladrow, D. A., R. E. Zeebe, C. Klaas, A. Körtzinger, and A. G. Dickson (2007), Total alkalinity: The explicit conservative expression and its application to biogeochemical processes, *Mar. Chem.*, *106*, 287–300.

Yang, Q., T. H. Dixon, P. G. Myers, J. Bonin, D. Chambers, M. van den Broeke, M. H. Ribergaard, and J. Mortensen (2016), Recent increases in Arctic freshwater flux affects Labrador Sea convection and Atlantic overturning circulation, *Nat. Commun.*, *7*(10525), doi:10.1038/ncomms10525.

Yasunaka, S., A. Murata, E. Watanabe, M. Chierici, A. Fransson, S. van Heuven, M. Hoppema, M. Ishii, T. Johannessen, N. Kosugi, et al. (2016), Mapping of the air–sea CO_2 flux in the Arctic Ocean and its adjacent seas: Basin-wide distribution and seasonal to interannual variability, *Polar Sci.*, *10*, 323–334.

Acknowledgments

I would like to acknowledge my first supervisor Dr. Morten Iversen for his time and patience for me between at least ten conferences and twenty cruises - I'm really impressed that for some people, days can have more than 24 hours. Thanks to Dr. Tim Rixen, who spontaneously agreed to be my second supervisor, even if Greenland fjords are a bit colder than his usual study areas. A big thank you goes to Dr. Mario Hoppema, who made it possible for me in the first place to join this cruise - thanks for the place in your office, for your day-to-day support, and the chances you gave me for my future career.

I deeply appreciate the support from a bunch of people helping me with the data analyses: Wilken-Jon von Appen for his oceanographic expertise; Anna Friedrichs, Helga van der Jagt, Bente Edvardsen, Jana Geuer, and Claudia Burau for providing me diverse datasets from the cruise; Anna Canning and Tobias Steinhoff from Geomar as well as Jens Herrmann from the "Wissenschaftlich-Technischer Dienst" of *Maria S. Merian* for giving me advices for the correction of the pCO_2 sensor data.

Many thanks to all the persons that saved me from getting crazy with all the different software and programs: Christian Konrad, Gerd Rohardt, and Antonia Immerz for their support with Matlab; Antonie Haas, Laura Hehemann and Anne-Cathrin Wölfl for helping me out with ArcGIS; Hauke Haake and my sister Maria for solving this and that LaTeX problem; Svenja Ryan for introducing me to Inkscape.

The cruise leader Boris Koch is to be thanked for a very enthusiastic and constructive collaborative expedition which was only possible due to his scientific passion. Thanks to the research group Physical Oceanography of Polar Seas from AWI ("die Ozis") for hosting me as a biologist and providing me with enough coffee and nice refreshing breaks in the morning. I'm especially thankful to Normen Lochthofen from the Deep Sea group at AWI for connecting me with Mario and for putting in a good word for me concerning several *Polarstern* cruises - I'm looking

forward to the next one.

I'm still moved by the big compassion of scientists and crew from MSM56 during my last days of the cruise. Whatever you did gave me a lot of power to weather the difficult time afterwards - I will never forget this!

I also would like to thank my friends for colouring my free time, for common relaxing and common facing of new challenges (what comes together with common freezing during winter evening runs).

Finally, the biggest thank goes to my family, who was supporting me mentally, financially, and with indispensable advices during my whole study. You are the most important persons in my life.

Universität Bremen

The following declarations are to be included in every exemplar of the Bachelor's and Master's Thesis

Name: Enrolment number:

Declaration of copyright

Hereby I declare that my Master's Thesis was written without external support and that I did not use any other sources and auxiliary means than those quoted. All statements which are literally or analogously taken from other publications have been identified as quotations.

Date: Signature

Declaration with regard to publishing theses

Two years after the final degree, the thesis will be submitted to the University of Bremen archive and stored there permanently.

Storage includes:

1) Master's Theses with a local or regional reference, as well as 10 % of all theses from every subject and year
2) Bachelor's Theses: The first and last Bachelor degrees from every subject and year

☐ I agree that for research purposes third parties can look into my thesis stored in the University archive.

☐ I agree that for research purposes third parties can look into my thesis stored in the University archive after a period of 30 years (in line with §7 para. 2 BremArchivG).

☐ I do not agree that for research purposes third parties can look into my thesis stored in the University archive.

Date: Signature